AD-A173 686 NEAR-WATER PROPAGATION EFFECTS AND MODERN SYSTEMS ADAPTATIONS(U) NAVAL OCEAN SYSTEMS CENTER SAN DIEGO CA J H RICHTER JUL 86 NOSC/TD-973 1/1

UNCLASSIFIED F/G 20/14 NL

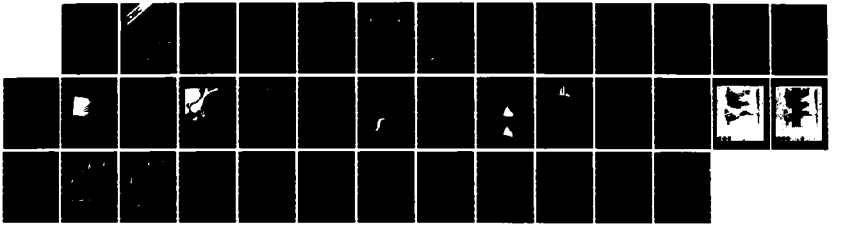

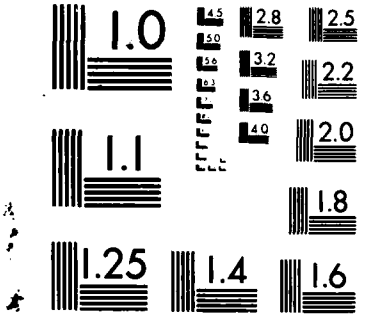

MICROCOPY RESOLUTION TEST CHART
NATIONAL BUREAU OF STANDARDS-1963-A

NOSC
OCEAN SYSTEMS CENTER San Diego, California 92152-5000

(12)

NOSC TD 973

Technical Document 973
July 1986

Near-Water Propagation Effects and Modern Systems Adaptations

J. H. Richter

AD-A173606

UNCLASSIFIED
SECURITY CLASSIFICATION OF THIS PAGE

REPORT DOCUMENTATION PAGE

1a. REPORT SECURITY CLASSIFICATION UNCLASSIFIED	1b. RESTRICTIVE MARKINGS
2a. SECURITY CLASSIFICATION AUTHORITY	3. DISTRIBUTION/AVAILABILITY OF REPORT Approved for public release; distribution is unlimited.
2b. DECLASSIFICATION/DOWNGRADING SCHEDULE	
4. PERFORMING ORGANIZATION REPORT NUMBER(S) NOSC TD 973	5. MONITORING ORGANIZATION REPORT NUMBER(S)
6a. NAME OF PERFORMING ORGANIZATION Naval Ocean Systems Center 6b. OFFICE SYMBOL (If applicable) Code 54	7a. NAME OF MONITORING ORGANIZATION
6c. ADDRESS (City, State and ZIP Code) San Diego, CA 92152-5000	7b. ADDRESS (City, State and ZIP Code)
8a. NAME OF FUNDING/SPONSORING ORGANIZATION Office of the Chief of Naval Research 8b. OFFICE SYMBOL (If applicable) OCNR-23	9. PROCUREMENT INSTRUMENT IDENTIFICATION NUMBER
8c. ADDRESS (City, State and ZIP Code) Arlington, VA 22217-5000	10. SOURCE OF FUNDING NUMBERS PROGRAM ELEMENT NO: 62759N PROJECT NO: RW 59551B TASK NO: N01A AGENCY ACCESSION NO: 540-SXB3

11. TITLE (Include Security Classification)
NEAR-WATER PROPAGATION EFFECTS AND MODERN SYSTEMS ADAPTATIONS

12. PERSONAL AUTHOR(S)
J. H. Richter

13a. TYPE OF REPORT	13b. TIME COVERED	14. DATE OF REPORT (Year, Month, Day)	15. PAGE COUNT
	FROM _____ TO _____	July 1986	41

16. SUPPLEMENTARY NOTATION

17. COSATI CODES			18. SUBJECT TERMS (Continue on reverse if necessary and identify by block number)
FIELD	GROUP	SUB-GROUP	Atmospheric physics; operations, strategy, and tactics; radar detection; propagation assessment; propagation tactics; electronic warfare; antiair warfare

19. ABSTRACT (Continue on reverse if necessary and identify by block number)

The Electromagnetic Wave Propagation Panel (EPP) of AGARD (Advisory Group for Aerospace Research and Development for NATO) has established a working group with the objective of assessing the effects of electromagnetic wave propagation along water surfaces for the entire electromagnetic spectrum from very low frequencies up to those in optical ranges. The working group is examining normal and abnormal propagation conditions with the aim of optimizing the performance of modern systems in communications, surveillance, and navigation, with special attention devoted to adaptive measures. This document is the author's contribution to the AGARD report covering the frequency range from 30 MHz--300 GHz.

20. DISTRIBUTION/AVAILABILITY OF ABSTRACT	21. ABSTRACT SECURITY CLASSIFICATION	
☒ UNCLASSIFIED/UNLIMITED ☐ SAME AS RPT ☐ DTIC USERS	UNCLASSIFIED	
22a. NAME OF RESPONSIBLE INDIVIDUAL J. H. Richter	22b. TELEPHONE (Include Area Code) (619) 225-7919	22c. OFFICE SYMBOL Code 54

DD FORM 1473, 84 JAN

83 APR EDITION MAY BE USED UNTIL EXHAUSTED
ALL OTHER EDITIONS ARE OBSOLETE

UNCLASSIFIED
SECURITY CLASSIFICATION OF THIS PAGE

CONTENTS

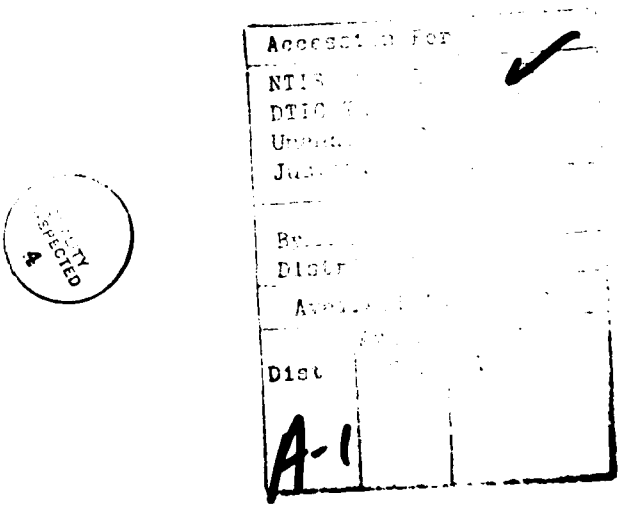

1. INTRODUCTION

In 1985, the Electromagnetic Wave Propagation Panel (EPP) of AGARD (Advisory Group for Aerospace Research and Development for NATO) established a working group under the title, "Near-Water Propagation Effects and Modern Systems Adaptation." The stated objectives were as follows:

"The Working Group will be concerned with the effects of electromagnetic wave propagation along water surfaces and within the entire electromagnetic spectrum from very low frequencies up to those in optical ranges. Normal and abnormal propagation conditions are to be examined with the aim of optimizing the performance of modern systems in communications, surveillance, and navigation. Special attention is to be paid to adaptive measures.

"In addition to an examination of the state of the art (e.g. NATO-DRG, Panel III – Activities) and to constructive conclusions with regard to feasible areas of future scientific research, development and engineering work, the final report is expected to contain detailed recommendations for such activities and also for operational measures, with the aim of adapting modern systems to special and detrimental features of near-water propagation effects."

The following is the author's contribution to the AGARD report covering the frequency range from 30 MHz to 300 GHz.

2. NEAR-WATER PROPAGATION EFFECTS AT VHF/UHF (30 MHz–3 GHz)

2.1 NORMAL PROPAGATION

The propagation of radio waves is influenced by the atmosphere's refractive index. The refractive index, n, of a parcel of air is defined as the ratio of the velocity of propagation of an electromagnetic (e.g., radar) wave in a vacuum to that in the air. Since electromagnetic (EM) waves travel slightly slower in air than in a vacuum, the refractive index is slightly greater than unity. At the Earth's surface, the numeric value of the refractive index n is usually between 1.000250 and 1.000400. To have a number that is easier to handle, the refractivity N has been defined to be $N = (n - 1) \times 10^6$, such that surface values of refractivity N vary between 250 and 400. Refractivity can be expressed as a function of atmospheric pressure, temperature, and humidity by the relation:

$$N = \frac{77.6P}{T} + \frac{3.73 \times 10^5 e}{T^2} \quad , \tag{2.1}$$

where

P is atmospheric pressure in millibars,

T is temperature in Kelvins, and

e is water vapor pressure in millibars.

For a well-mixed "standard" atmosphere, temperature, humidity, and pressure decrease with altitude, such that N decreases with height at a rate of about 39 N units per 1000 meters (or 12 N units per 1000 ft). The behavior of an EM wave propagating horizontal to the Earth's surface is such that it will bend or "refract" toward the region of

higher refractivity (lower velocity). For the standard atmosphere, a radar wave will bend down toward the Earth's surface, but with a curvature less than the Earth's, as shown in figure 2.1.

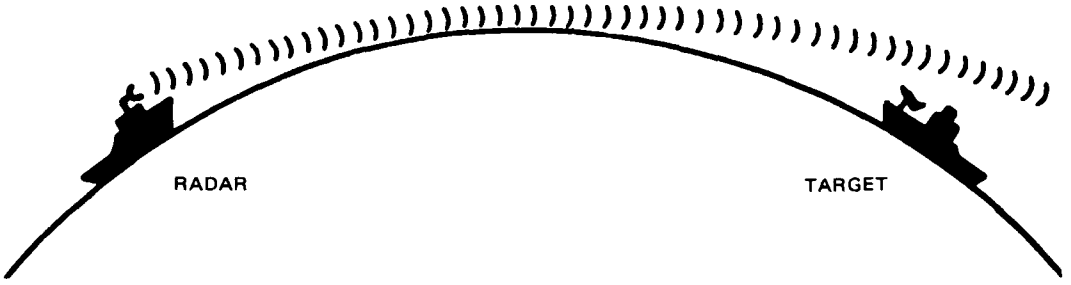

Figure 2.1. Radar wave path under "standard" atmospheric conditions. Note that the path curves downward, but at a rate less than that of the Earth's curvature.

The refractive index is nondispersive, and bandwith limitations are generally not encountered.

If an EM wave is propagating from a transmitter to a receiver (or target), and both the transmitter and receiver are sufficiently far removed from the Earth or other objects, the EM wave is said to be propagating in free space. Let P_t be the power transmitted and P_r be the power received. Then the path loss (or propagation loss) between the transmitter and receiver, in decibels, is defined to be

$$L = 10 \text{ Log}_{10} \frac{P_t}{P_r} . \tag{2.2}$$

In free space, the path loss is determined by the geometrical spreading of the power over the surface of the expanding sphere centered at the transmitter and is given by

$$L_{fs} = 37.8 + 20 \text{ Log}_{10} f + 20 \text{ Log}_{10} R \tag{2.3}$$

where f is the transmitter frequency in MHz and R is the range between the transmitter and receiver in nmi. Equation 2.3 assumes that both the transmitter and receiver employ lossless isotropic (radiating uniformly in all directions) antennas. L_{fs} would be a good approximation for path loss between two aircraft, if both aircraft were at reasonably high altitudes and there were no elevated ducts present near their altitudes. However, for a transmitter or receiver near the surface, reflections from the surface must be taken into account.

Reflection and the Interference Region

When an EM wave strikes a nearly smooth large surface, such as the ocean, a portion of the energy is reflected from the surface and continues propagating along a path that makes an angle with the surface equal to that of the incident ray, as illustrated by figure 2.2. The strength of the reflected wave is determined by the reflection coefficient, which depends on the frequency and polarization of radiation, the angle of incidence, and the roughness of the reflecting surface disturbed by the wind. Not only is the magnitude of the

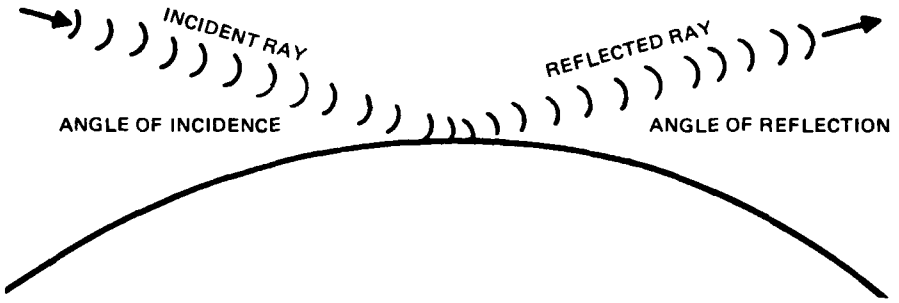

Figure 2.2. Incident ray and reflected ray illustrating equal angles of reflection.

reflected wave reduced, but the phase of the EM wave is also altered. Typical values for the reflection coefficient for shallow incidence angles and smooth seas are 0.99 (i.e., the reflected wave is 99 percent as strong as the incidence wave) and 180 degrees of phase change.

As the wind speed increases, the ocean surface grows rougher and the reflection coefficient can decrease to about 0.15 (the phase change is unaffected). For a transmitter near the surface, the reflection process results in two paths to a receiver (or target) within line of sight, as illustrated by figure 2.3. As the geometry changes in figure 2.3, the relative lengths of the direct path and the reflected path also changes, which results in the direct and reflected waves arriving at the receiver with varying amounts of phase difference. The received signal strength is the vector sum of the signal strengths of the direct and reflected wave, which causes the received power to vary up to 6 dB above and up to 20 dB or more below the free-space value.

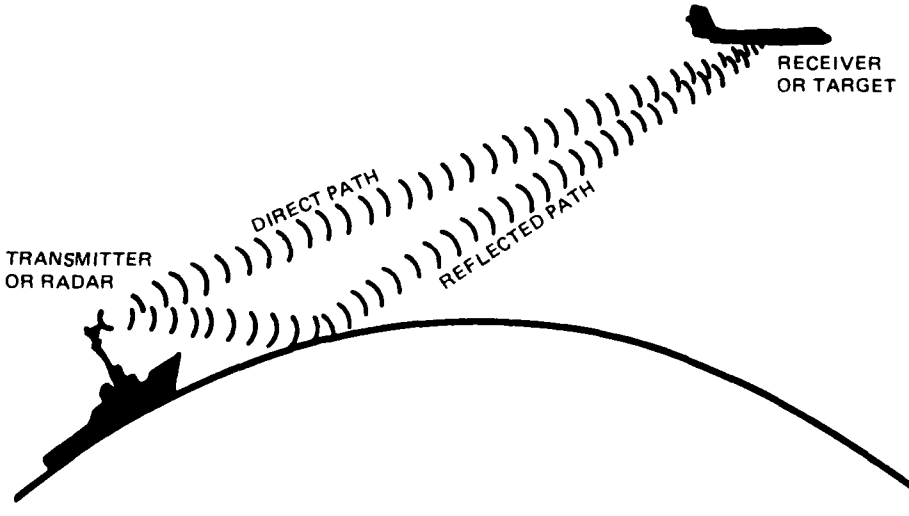

Figure 2.3. Surface-to-air geometry illustrating direct and sea-reflected paths.

Figure 2.4 shows a plot of path loss versus range for a 5000-MHz (5-GHz) transmitter located 60 feet above the sea surface and a receiver at 100 feet above the sea surface for standard refractive conditions. The region in which the path loss is dominated by the interference of the direct and sea-reflected wave is called the interference region and is labeled as such in figure 2.4. The free-space path loss, as calculated from equation 2.3, is included in figure 2.4 for reference and illustrates how the path loss oscillates above and below the free value in the interference region. The depth of the nulls depends very much on the surface roughness related to the wind speed. The example here is for a smooth sea surface associated with zero wind speed, but as the wind speed increases the path loss in the nulls would approach the free-space value.

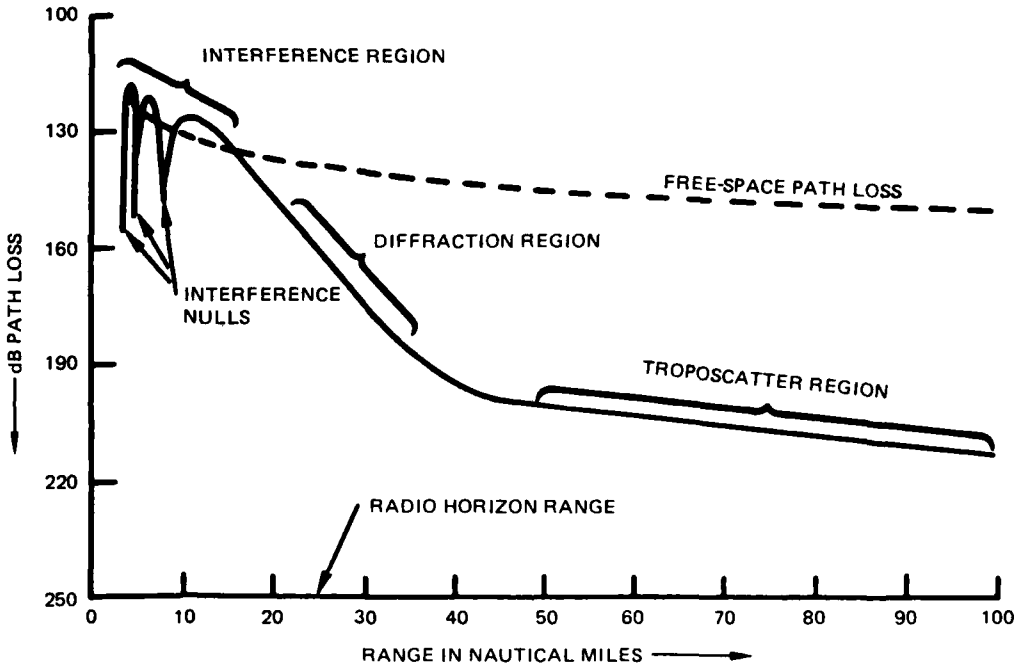

Figure 2.4. Path loss curve for a 5000-MHz transmitter at 60 ft and a receiver at 100 ft for a standard atmosphere.

Diffraction

Near the radio horizon range, where the path between the transmitter and receiver is just tangent to the Earth's surface, the path loss is dominated by diffraction around the Earth. The diffraction region, which is sometimes called the shadow region, is characterized by propagation beyond the line-of-sight or radio horizon because of the ability of a radio wave to travel along an interface of dissimilar materials, in this case the Earth's surface and the atmosphere. The amount of power, or signal strength, available to a receiver in this region is very dependent on the refractive conditions near the Earth's surface. In fact, the various forms of ducting to be described in the following sections are actually special cases of propagation in the diffraction region. To calculate path loss in the diffraction region, in any case, is very complicated and is usually based on notions of normal-mode propagation and atmospheric waveguide considerations.

Tropospheric Scatter

At ranges far beyond the horizon, the path loss is dominated by a mechanism called tropospheric scatter or troposcatter (figure 2.4). Propagation in the troposcatter region is the result of scattering of the EM wave from refractive heterogeneities at relatively high altitudes, which are line-of-sight to both the transmitter and receiver. The calculation of path loss in the troposcatter region is quite easily performed by using semiempirical formulations. The rate at which the path loss increases with range, within the troposcatter region, is considerably less than the rate in the diffraction region (figure 2.4). However, the path loss values found in this region are so high that it is impossible for any known radar system to detect targets. Troposcatter is an important consideration for certain communications systems and ESM receivers.

Absorption

A standard propagation mechanism that was not illustrated in figure 2.4, but should be mentioned, is absorption. Oxygen and water vapor molecules in the atmosphere absorb some energy from radio waves and convert it to heat. The amount of absorption is highly dependent on the radio frequency and is negligible, compared to all the other propagation considerations, below 20 GHz. Absorption by rain drops and other forms of precipitation can be important, and may be estimated from curves found in standard textbooks like Skolnik (1980). Since the refractive index in this frequency range is nondispersive, bandwidth limitations are usually not encountered.

2.2 ANOMALOUS PROPAGATION

Anomalous propagation mechanisms are all associated with abnormal distributions of the refractive index. If the refractivity gradient exceeds 0 N/km, a radio ray will bend upwards and the layer is said to be subrefractive and has the effect of shortening the horizon. If the gradient is between -157 and -79 N/km, the ray will still bend downwards at a rate less than the Earth's curvature but at a rate greater than standard. These gradients are called superrefractive and have the effect of extending the horizon. The most dramatic nonstandard effects are those caused by gradients less than -157 N/km, which are called trapping gradients. In this case, the ray curvature exceeds the Earth's curvature and leads to the formation of ducting, which can result in propagation ranges far exceeding the normal horizon. The modified refractivity M is defined by $M = N + (h/a) \times 10^6 = N + 0.157h$, where h is height in meters and a is the Earth's radius in meters. M is useful in identifying trapping gradients, in that trapping occurs for all negative M gradients. Table 2.1 lists the four refractive conditions discussed above and their relation to N and M gradients, and figure 2.5 illustrates the relative curvature for each.

Table 2.1. Four refractive conditions and their relation to N and M gradients.

Condition	N-Gradient (N/km)	M-Gradient (M/km)
Trapping	$dN/dh \leq -157$	$dM/dh \leq 0$
Superrefractive	$-157 < dN/dh \leq -79$	$0 < dM/dh \leq 78$
Standard	$-79 < dN/dh \leq 0$	$78 < dM/dh \leq 157$
Subrefractive	$dN/dh > 0$	$dM/dh > 157$

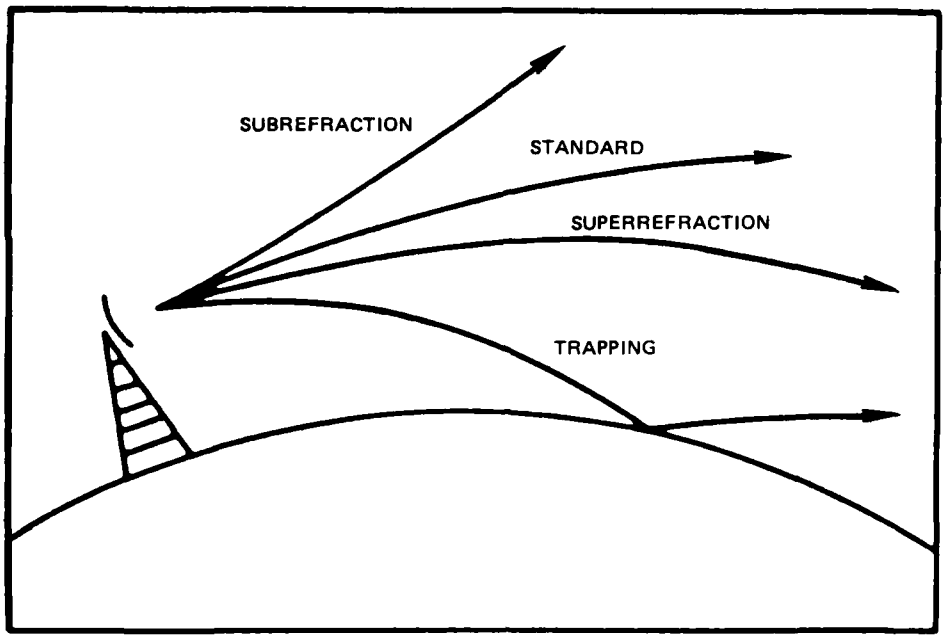

Figure 2.5. Relative bending for each of the four refractive conditions.

In a marine environment, there are three distinct types of ducts caused by trapping gradients; namely, surface-based ducts, elevated ducts, and evaporation ducts. Surface-based ducts are usually created by trapping layers that occur up to several hundred meters in height, although they can be created by a trapping layer adjacent to the surface (sometimes referred to as simply surface ducts). Figure 2.6 shows the N and M profiles for a typical surface-based duct. The condition for a surface-based duct to exist is that the M value at the top of the trapping layer be less than the M value at the surface. These ducts are not particularly sensitive to frequency, being able to support long over-the-horizon propagation ranges at frequencies above 100 MHz. Surface-based ducts occur with annual frequencies of up to 50 percent in areas such as the Eastern Mediterranean and Northern Indian Ocean, and are the type of duct responsible for most reports of extremely long over-the-horizon radar detection and communication ranges.

Elevated ducts are created by elevated trapping layers of the same type as those that create most surface-based ducts. However, in this case, the layer is either too high or the M deficit across the trapping layer is too small to meet the condition previously stated to form a surface-based duct. Figure 2.7 illustrates the N and M profiles required for an elevated duct. The vertical extent of the duct is from the top of the trapping layer down to a height where the M value is equal to the M value at the top of the trapping layer. Elevated ducts can also affect propagation for frequencies above approximately 100 MHz, but the effects are usually limited to airborne emitters or sensors located close to or above the elevated duct. The primary effects are extended ranges for receivers or targets within the duct and radio or radar "holes" in coverage for receivers or targets at altitudes above the duct. Elevated ducts occur at altitudes up to about 6 km, although they are most common below 3 km. Again, since the refractive index is nondispersive, bandwidth limitations are usually not encountered.

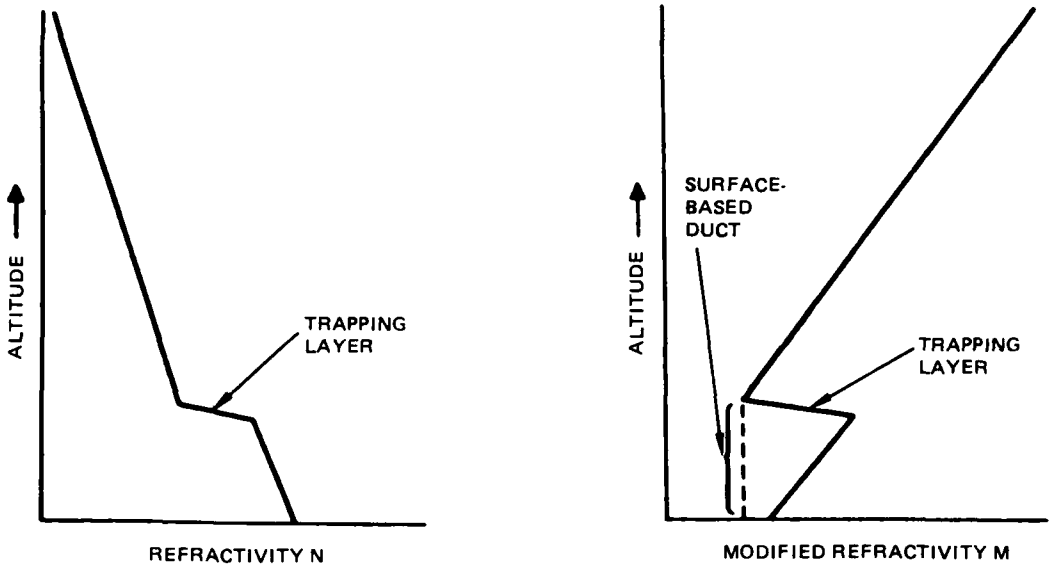

Figure 2.6. N and M profiles for a surface-based duct.

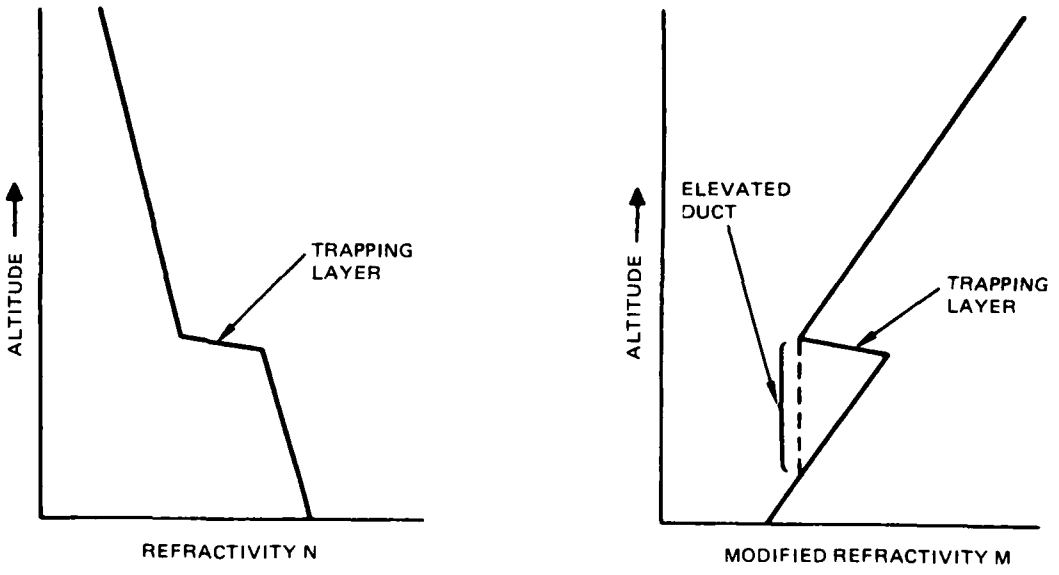

Figure 2.7. N and M profiles for an elevated duct.

2.3 DATA GAPS TO BE FILLED

Worldwide radiosonde measurements provide the basis for extensive climatologies of marine atmospheric effects (Patterson, 1982). Helvey (1983) pointed out some systematic errors and how they may be minimized. For some applications, these systematic errors may consititute a data gap that needs to be filled.

Surface roughness and radar clutter can generally be handled satisfactorily under standard atmospheric conditions. Under ducting conditions, radar clutter may be significantly enhanced. Almost no radar clutter data under ducting conditions with associated refractivity profiles exist, which is the reason that modeling of this phenomenon is very limited. Also absent from most propagation measurements are good fading statistics, which are important for some applications like inverse synthetic-aperture radar over-the-horizon imaging capability under ducting conditions.

Perhaps the most serious reason for data gaps are the limitations in refractivity-sensing techniques. For propagation assessment purposes, the vertical profile of radio refractivity should be known to within one N unit, with a vertical resolution of less than 10 m. The best instrument for measuring atmospheric refractivity is a microwave refractometer. It measures radio refractivity directly, with excellent accuracy and response time. It must be carried by aircraft or balloon for vertical profiling and is relatively costly and electronically complex. Many versions are in use today, including one on a US Navy aircraft carrier-based airplane. The most commonly used instrument for measuring atmospheric refractivity is still the radiosonde. It measures temperature and humidity as a function of pressure. Radio refractivity and altitude are calculated from those values. The calculated refractivity profile is generally satisfactory if sufficient care in calibration and data reduction is taken. One particular problem with radiosonde-deduced surface ducts has been pointed out and analyzed by Helvey (1983) and concerns erroneous surface-based ducts resulting from limitation in the response time of the sensors and in data-reduction procedures. This problem is particularly troublesome for refractivity climatologies based on archived standard radiosonde data. The most desirable instrument for measuring atmospheric refractivity would be based on a remote-sensing technique, preferably passive. Unfortunately, water vapor profiles obtained with microwave radiometers do not have the vertical resol. .on needed. Active remote sensors using microwave radar sense refractivity fluctuations associated with mixing across gradients in the vertical refractivity profile (Richter, 1969). The relationship between those fluctuations and gradients is presently the subject of intense investigation (Gossard et al., 1982). Two lidar techniques (differential absorption or DIAL, and Raman scattering) have been used for measuring water vapor and temperature profiles. They will, however, not work under cloudly conditions that severely limit their general usefulness for refractivity applications. Reception of signals from known emitters, either ground- or satellite-based, may be used to sense the propagation medium. In this way, conditions along the entire propagation path of interest for the desired frequency can be sensed directly. However, only in rare cases will it be feasible to have a source at the right frequency and location. Inferring the vertical refractivity structure itself along the path requires multifrequency signals and complex profile inversion schemes. Use of beacons from satellites passing through the horizon has been recently analyzed by Anderson (1982). This technique relates shifts in interference null location with vertical refractivity structure. The practical utilization of this technique, however, is limited by signal fluctuations caused by random inhomogeneities of the medium. Averging times required for precise measurements of interference patterns are too long for the relatively short time a satellite passes through the horizon.

Some qualitative radio propagation inferences may be drawn from satellite-sensed cloud patterns, usually in conjunction with weather charts. Well mixed atmospheric conditions will generally indicate standard propagation conditions, while stratifications may indicate the possibility of ducting.

Propagation assessment is usually based on one refractivity profile measured along a slant path in the vicinity of the propagation path as close as possible to the time of interest. The underlying assumption is that the atmosphere is horizontally stratified to justify use of a single profile for propagation calculations. This assumption is based on a physical reason since the atmosphere, in particular over ocean areas, is horizontally much less variable than vertically. Horizontal stratification also implies temporal persistence. Propagation forecasts are often based on persistence; i.e., it is assumed that present conditions will not change significantly in the near future. There are, however, conditions for which horizontal inhomogeneity may be important; for example, at air mass boundaries or in coastal regions. The question is how often horizontal inhomogeneity must be considered for valid propagation assessment. For this purpose, simultaneous refractivity and propagation data were examined (Glevy, 1976). It was found that calculations of propagation enhancements based on a single profile were correct in 86 percent of the cases. A similar conclusion has been reached from 5 years of shipboard experience with IREPS.

Propagation assessment would be considerably more complicated and costly if effects of horizontal inhomogeneity must be included. In this case, refractivity has to be sensed at multiple locations and more frequently since persistence is no longer a valid assumption. This would require an increase of the number of refractivity profile soundings by roughly an order of magnitude (for reliable shipboard propagation assessment, presently one to two radiosonde soundings are taken in each 24-hour period). Propagation calculations are more complex for inhomogeneous paths and are azimuth-dependent. In addition, they must be performed more frequently. One may assume that horizontal inhomogeneity is responsible for part of the 14 percent of incorrect assessments mentioned before, and that their proper assessment would reduce this number by one-half. Then the expected improvements in routine propagation assessment would be only about 4 percent for those areas with the greatest occurrence of surface-based ducts of around 50 percent, and much less for areas where ducting is uncommon. Consideration of horizontal inhomogeneity effects depends, therefore, on a tradeoff between the improvement in propagation assessment accuracy and cost, and must be decided on a case-by-case basis.

Refractivity forecasting requires very accurate prediction of the atmospheric humidity profile and its dynamic behavior. Refractive boundary layer structures have been modeled by Burk (1977, 1980) and Gossard (1977, 1980). However, for operational purposes, refractivity forecasts (other than persistence) are qualitative. For example, a high-pressure ridge and associated subsidence may produce ducting layers, and a well-mixed atmosphere will probably indicate standard propagation conditions. Satellite imagery of clouds can be used for similar qualitative statements of ducting conditions.

2.4 SYSTEMS APPLICATIONS

For radars, surface-based ducts offer the possibility of greatly extended detection (but also intercept) ranges. A famous example is the World War II sighting of Arabia with a 200-MHz radar from India 1700 miles away (Freehafer, 1951). Similarly, under surface ducting conditions, communication ranges may be greatly extended. However, the major applications for naval systems is in the electronic warfare (EW) area. Emission control or

EMCON requires a good knowledge of how far away signals may be intercepted. Therefore, any sensible EMCON planning must take anomalous propagation effects (i.e., primarily extended ranges under surface ducting conditions) into account. Another EW discipline seriously affected by propagation anomalies is jamming. Jamming effectiveness may be increased significantly by placing the jammer in such a way that optimum propagation conditions are utilized.

2.5 SYSTEMS ADAPTATIONS

One method for assessing how EM shipboard systems performance is affected by propagation anomalies is the Integrated Refractive Effects Prediction System (IREPS) described originally by Hitney and Richter (1976), and more recently by Hattan et al. (1983). IREPS is designed primarily for use aboard naval ships to assess and exploit changes in the coverage patterns of radar, electronic warfare, and communications systems caused by abnormal refractivity structures in the lower atmosphere. The system is based around a Hewlett-Packard 9845 desk-top computer and uses the propagation models presented in sections V and VI of Hitney et al. (1985), except that no provision for horizontal changes in refractivity structure is included. Other limitations include the use of only ray optics for air-to-air geometries, as opposed to full-wave solutions, and an approximate single-mode waveguide for surface-based ducts. The environmental input is primarily from radiosondes, and consists of pressure, temperature, and relative humidity, although the capability exists to interface IREPS with recordings from airborne microwave refractometers when they are available. The propagation models will handle a wide variety of surface-based and air-borne air-search radars, some surface-search radars, and several electronic warfare and communications systems. The frequency limits of the system are 100 MHz to 20 GHz.

An example of an IREPS display is shown in figure 2.8. This example is for a hypothetical 400-MHz air-search radar with the radar antenna height being 100 ft above sea level. The display shows this radar's coverage on a spherical Earth range-versus-altitude diagram, with three shaded regions that correspond to 90-, 50-, and 10-percent probabilities of detection of a small airborne target, based on free-space detection ranges of 46, 73, and 100 nmi. This example is for a refractivity structure characterized by a surface-based duct extending up to about 300 miles, which results in the extended ranges indicated in the figure near the surface. At higher altitudes, the example shows three of the normal interference lobes, where their location has been modified from the standard atmosphere case based on ray traces through the actual refractivity profile. Only the first three of the lobes are shown, since higher ones get closer together and are both harder to resolve on the display and less meaningful to a user.

In addition to the coverage display, IREPS will generate path-loss-versus-range displays that can be used in assessing maximum range performance for radar, communications, or electronic warfare applications when both terminals are located at fixed heights above the water. There are also tables that can be generated to assess maximum expected detection ranges of surface-search radars against predefined sets of ship classes, or to assess maximum expected intercept ranges of predefined sets of radar emitters. Finally, there are displays that show the refractivity structure, and give general assessments of propagation conditions, based on either *in situ* measurements or stored climatologies.

IREPS can be and is used for tactical decision aids. An example is shown in figure 2.9 for stationing of an attack aircraft. An enemy radar detection envelope under standard atmospheric conditions is schematically depicted on the left side. The optimum

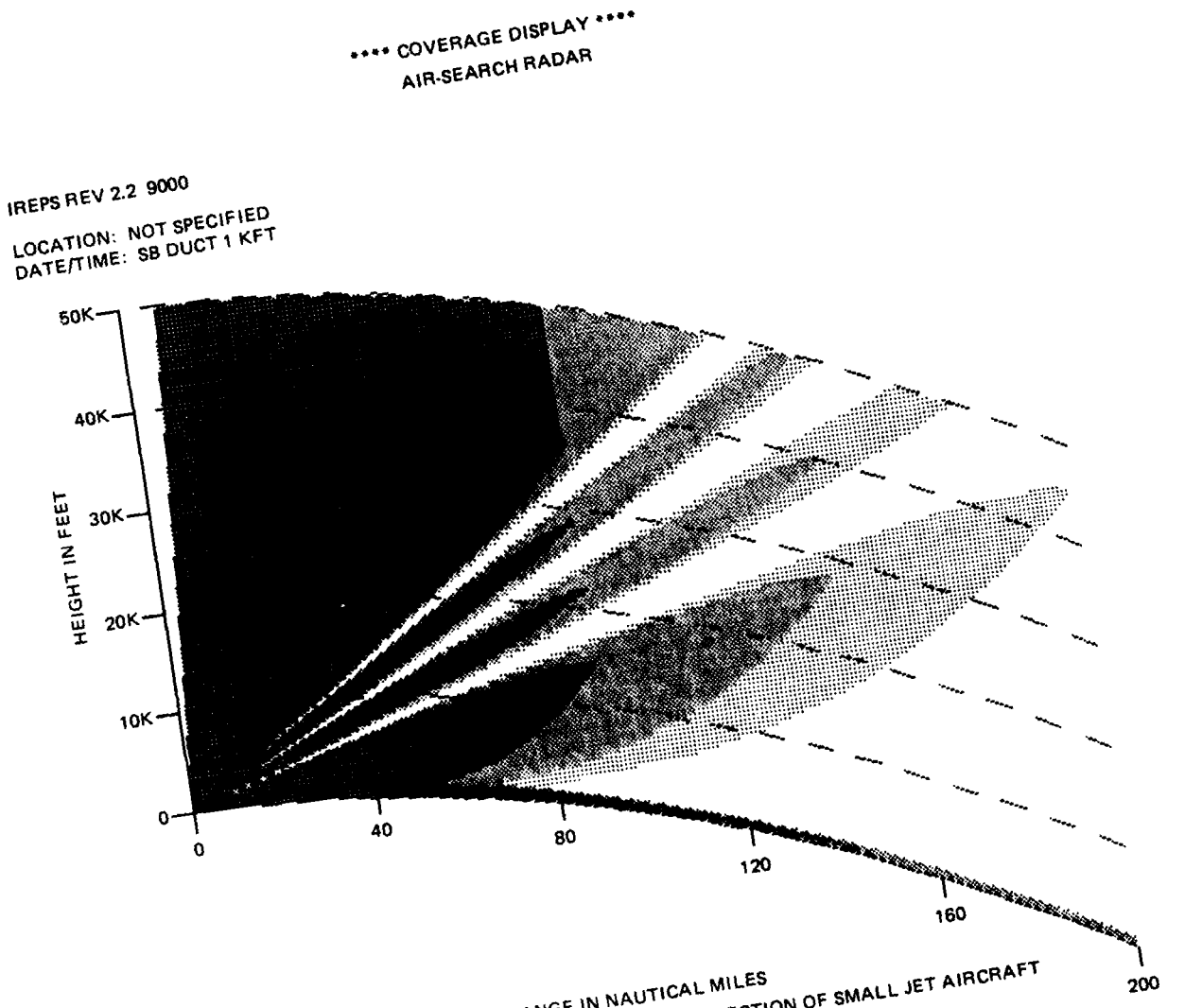

Figure 2.8. Example of a coverage display from IREPS.

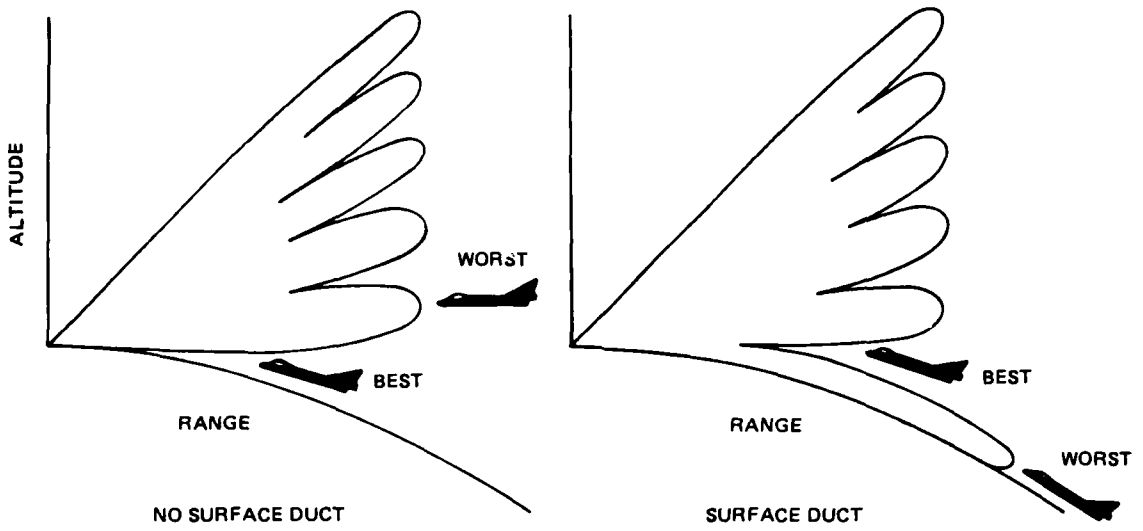

Figure 2.9. Typical IREPS radar coverage diagrams and attack aircraft positions.

attack aircraft flight altitude for minimizing detection is as close to the ocean surface as possible, which is the commonly used approach. However, under surface ducting conditions, the radar's detection range is greatly extended (right side). Under these conditions, a low-flying aircraft would be detected at otherwise unexpectedly long ranges. If the aircraft flies just above the surface duct, as indicated on the right side, it minimizes detection by the radar. This specific tactic has been proven under operational conditions and is commonly used on aircraft carriers equipped with IREPS.

Another more complex example of a TDA is shown in figure 2.10. The display shows the planned route of a battle group for a 3-day period. The shaded areas around the track show the 50-percent and 90-percent probability of intercept ranges a hostile intercept receiver would achieve against the combined radio and radar emitters of the battle group. The propagation ranges are based on environmental forecasts provided either centrally or locally from local area forecast models.

Problems associated with systems adaptation to near-water propagation effects are correct and timely sensing of refractivity, horizontal extent (homogeneity) of refractive layers, and forecasting of refractive structures. In addition, it is difficult to interface the proper environmental information with the already high complex command and control (C^2) process.

Despite present difficulties and shortcomings, the trend is clearly toward a comprehensive propagation assessment capability, including the development of more TDAs. Exploitation and mitigations of anomalous propagation effects is clearly becoming an integral part of future C^2 systems.

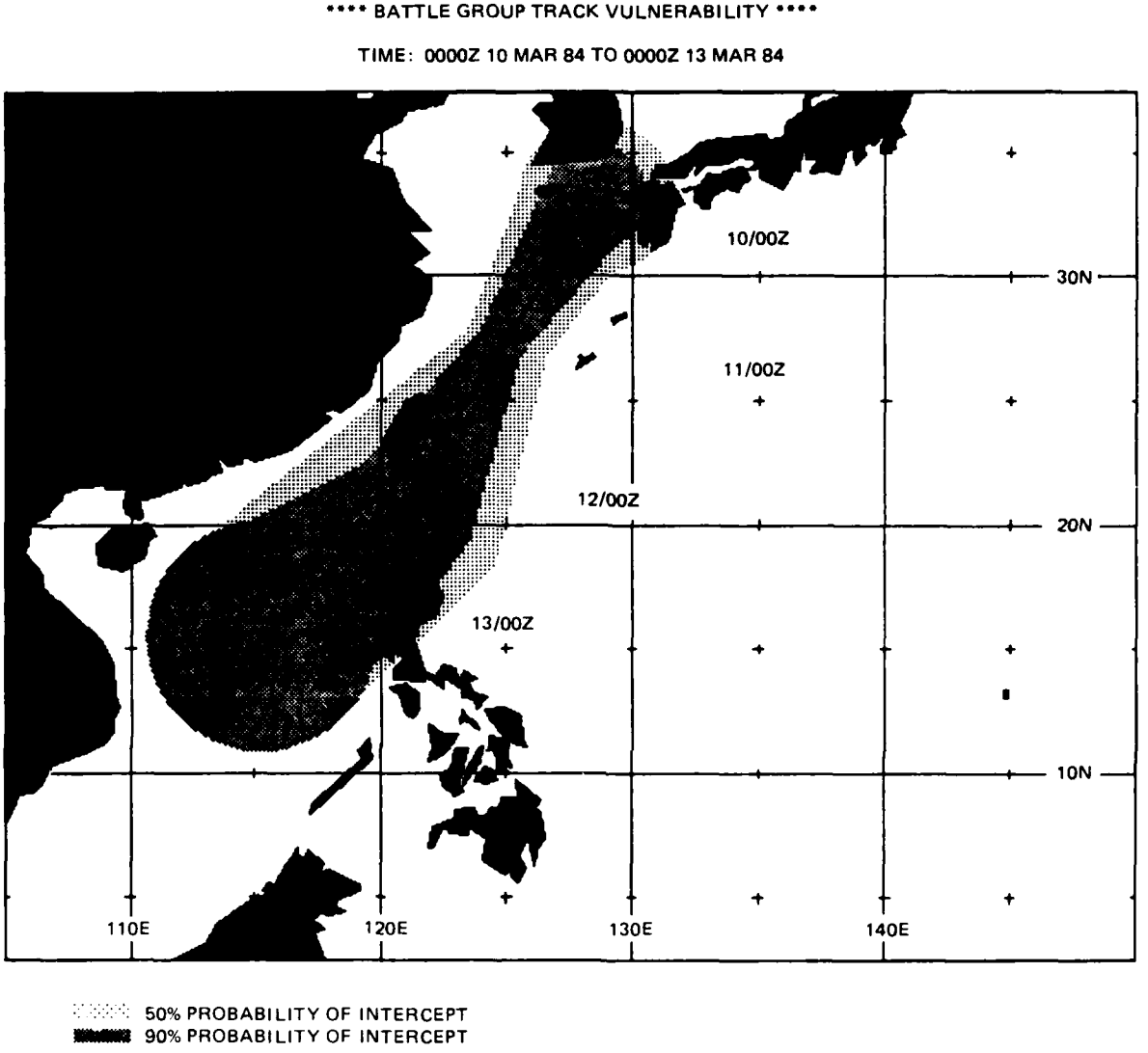

Figure 2.10. An example of vulnerability of a battle group along a track.

3. NEAR-WATER PROPAGATION EFFECTS ON SYSTEMS AT SHF (3–30 GHz)

3.1 NORMAL PROPAGATION

The propagation mechanisms described in section 2.1 also hold for the SHF (3–30-GHz) band. In addition, water vapor absorption and attenuation by rain become increasingly important. Figure 3.1 illustrates the influence of both effects for frequencies above 10 GHz. The first gaseous resonance (from water vapor) occurs around 22 GHz. Rain, depending on its intensity, may be a serious attenuating mechanism.

Bandwidth limitations are generally not encountered throughout this frequency range (even in the vicinity of 22 GHz, where the dispersion of the refractive index would be

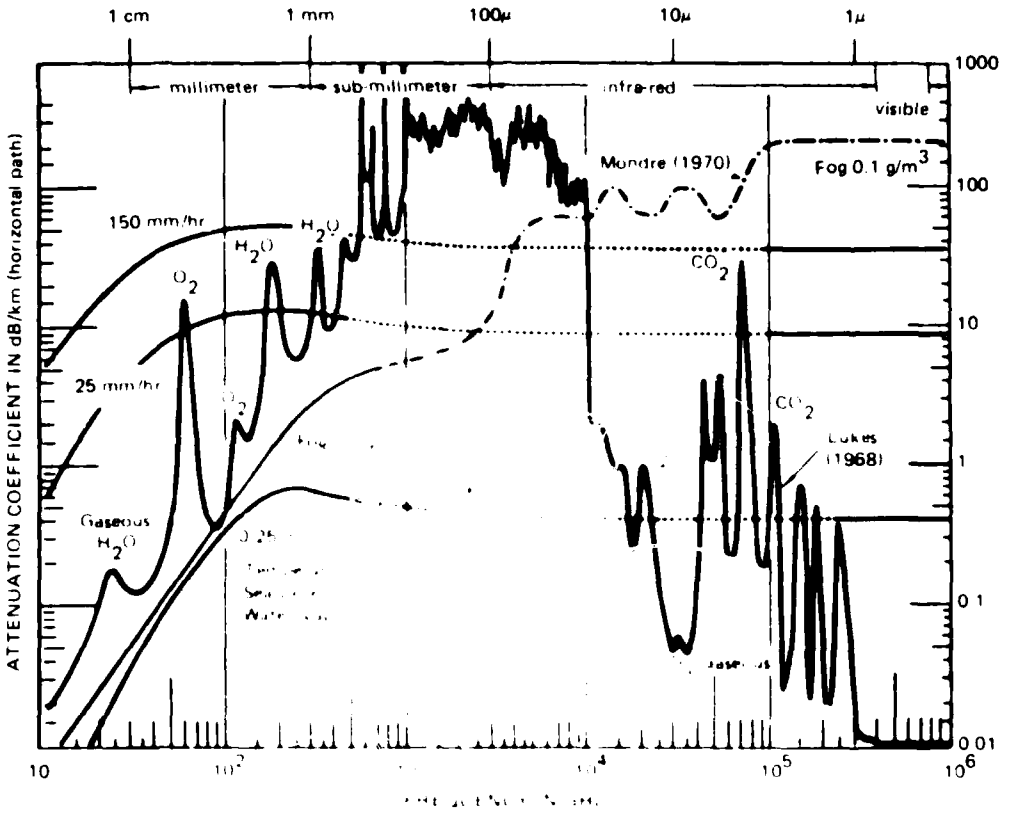

Figure 3.1. Attenuation due to gaseous constituents and precipitation for transmission through the atmosphere (CCIR Document 5/142-E).

expected to be the greatest). Multiple scattering in rain can also limit the bandwidth of incoherent transmissions because of the variation in time delays of multiple scattered signals; however, attenuation under such conditions will present a far more serious problem. A study of the problem of bandwidth limitations imposed by the frequency dependence of attenuation and the phase shift resulting from rain on coherent transmission systems showed that such bandwidth limitations are in excess of 3.5 GHz for all situations likely to be encountered (Crane, 1967).

3.2 ANOMALOUS PROPAGATION

The propagation anomalies described in section 2.2 also apply to the SHF band. In addition, over the ocean another important and persistent ducting mechanism is encountered: the oceanic evaporation duct. This is a nearly permanent propagation mechanism created by the very rapid decrease of moisture immediately above the ocean surface. For continuity reasons, the air adjacent to the ocean is saturated with water vapor and the relative humidity is thus 100 percent. This high relative humidity decreases rapidly with increasing height in the first few meters until an ambient value is reached that depends on general meteorological conditions. The rapid decrease in humidity creates a trapping layer adjacent to the surface, as illustrated by the modified refractivity curve in figure 3.2. The

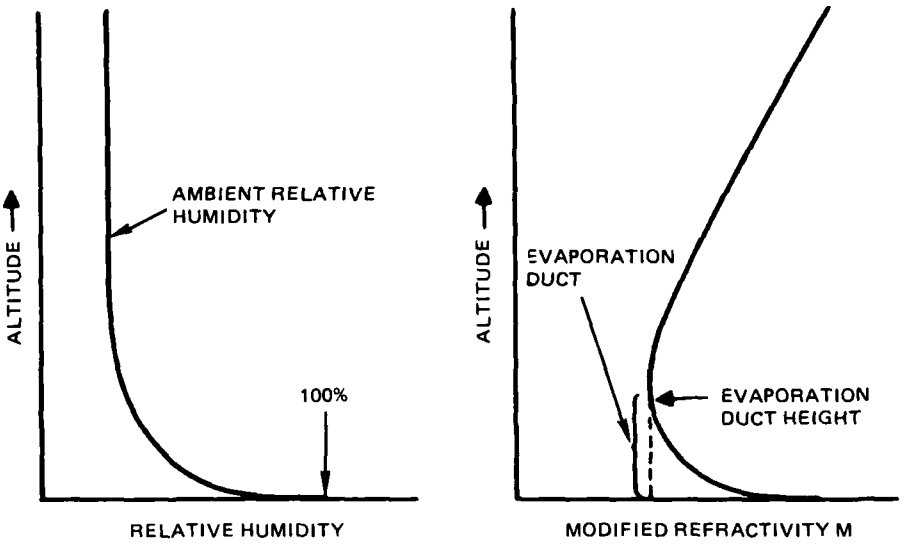

Figure 3.2. Relative humidity and M profiles for an evaporation duct.

height at which a minimum value of M is reached is called the evaporation duct height, which is the measure of strength of the duct. The evaporation duct itself extends from the duct height down to the surface, but because evaporation ducts are very "leaky," they affect radio and radar terminals significantly above as well as within the duct. The frequencies that the evaporation duct can affect are strongly dependent on the existing duct height, with a lower practical limit of about 3 GHz. The evaporation duct heights vary generally between 0 and 40 m, with a long-term mean value of about 8 m at northern latitudes and up to about 30 m at tropical latitudes. The primary evaporation duct effects are to give extended ranges for surface-to-surface radio or radar systems operating above 3 GHz. The optimum frequency to achieve extended ranges via the evaporation duct appears to be around 18 GHz (Richter and Hitney, 1975; Anderson, 1982, 1983). Although the ducting effect extends beyond this frequency, absorption by atmospheric gases and extra attenuation resulting from a rough sea surface begin to counteract the benefits of the duct.

The theoretical framework for calculation of evaporation duct height is proposed by Monin and Obukhov (1954) and is based upon the relation of surface layer profiles of temperature, moisture, and turbulence with surface fluxes of momentum, sensible heat, and latent heat. Multilevel measurements needed to determine these surface fluxes are extremely difficult and are operationally beyond the capability of field meteorologists. For this reason, a "bulk" measurement method is sought. If the Monin-Obukhov expressions for temperature, moisture, etc., are expressed as mathematical derivatives, the integral from a rough surface boundary (z_o) to some reference height (z) will express the fluxes. This introduces two integration boundary conditions. By making certain assumptions about the meteorological conditions at z_o, only the four variables of air temperature (T_a), sea-surface temperature (T_s), moisture (Rh), and wind velocity (U), all measured at z, and the determination of z_o need to be made to determine these fluxes. These meteorological measurements then are referred to as "bulk" measurements.

Two commonly used models by Jeske (1971) and Rotheram (1977) rely on "bulk" meteorological measurements to calculate a refractive difference between z and z_o, a scale

length empirically derived from the bulk Richard's number, and a profile coefficient. Based on two empirically derived stability functions, the refractive difference and the scale length are used to explicitly calculate duct height. An evaluation by Patterson (1985) concluded that both models produce similar results. Duct height, however, is critically dependent on the knowledge of the air-sea temperature difference to an accuracy of a few tenths of 1 degree. As one would expect, individual measurements under operational conditions rarely meet these accuracy requirements. Consequently, individual duct height calculations show large variances, as do the path loss calculations based on them. In a statistical sense (assuming there is no bias in the measurements), duct height and associated path loss calculations have given satisfactory results, specifically when recently developed correction methods have been applied (Paulus, 1985). An example of comparisons of measurements with waveguide calculations, using Paulus' (1985) duct height corrections, is shown in figure 3.3. The data in this figure consisted of measurements of path loss at 18 GHz over an 81-km path between San Nicolas and San Clemente Islands off the coast of California in June 1982. Transmitter and receiver antennas were situated at 19 and 11 m, with a horizon range of 32 km. Thus the propagation path extended 2.5 times the horizon range. Concurrent meteorological measurements consisted of continuously measured surface data at San Clemente Island and twice-daily radiosonde measurements at both San Clemente and San Nicolas Islands.

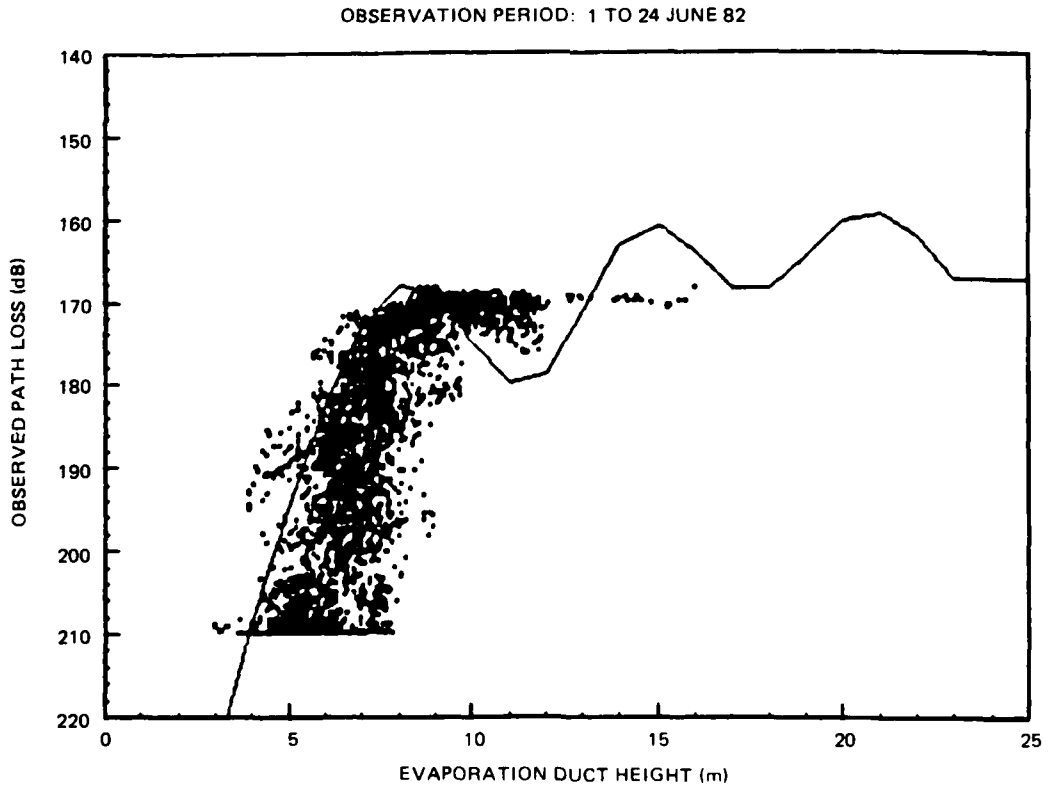

Figure 3.3. Comparison of measured (dots) and calculated (solid line) path loss values for an 18-GHz, 81-km over-water path (Paulus, 1985).

An extensive set of evaporation ducting measurements was conducted in the Southern California off-shore area, the Mediterranean, and the Caribbean (Richter and Hitney, 1972; Richter and Hitney, 1973; Richter et al., 1973; Richter and Hitney, 1975; Anderson et al., 1974). An example of 9.4-GHz path loss measurements over a 35-km path (5-m terminal heights) between the islands of Mykonos and Naxos in the Aegean Sea is shown in figure 3.4(a) (solid line). Path loss values calculated from meteorological data measured at one site are indicated by dots. Agreement between measured and calculated data is reasonable considering the contamination of the duct height data from shore effects. Signal enhancements exceeding free-space values are not uncommon.

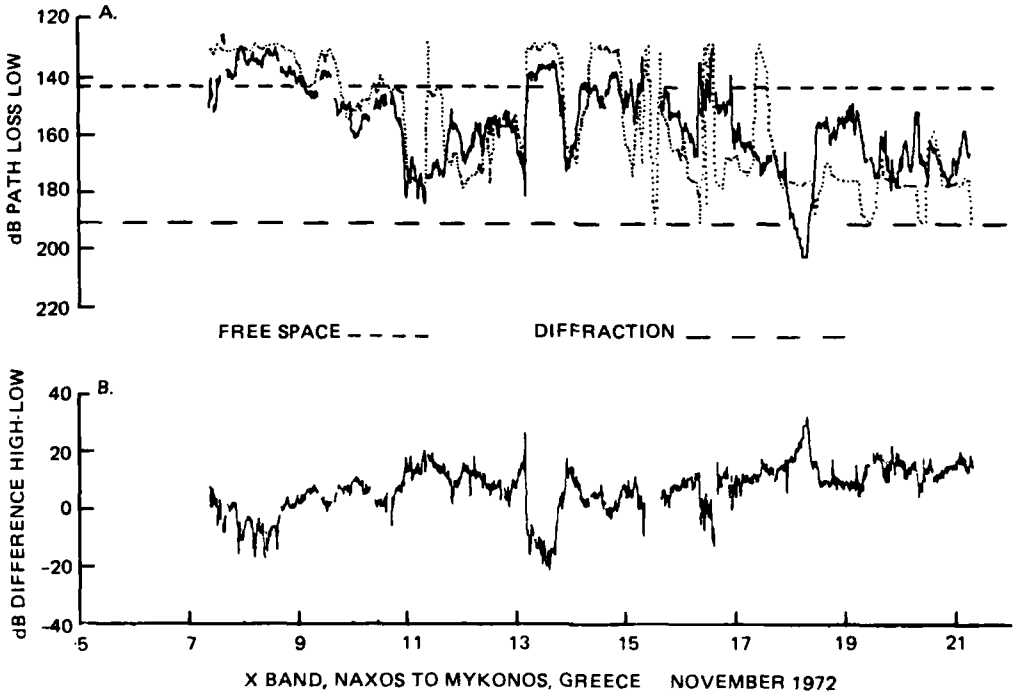

Figure 3.4. (a) Calculated (dotted) and observed path loss data for 9.6 GHz; (b) Observed difference between antennas at 5 and 20 m versus time.

3.3 DATA GAPS TO BE FILLED

In addition to the data gaps discussed in section 2.3, better evaporation ducting data are needed. Reliable open-ocean evaporation duct measurements are very scarce and measurements in coastal areas are few. A significant improvement of worldwide evaporation duct statistics is expected by applying Paulus' (1985) correction technique to presently available statistics. Accordingly, an update of the Naval Ocean Systems Center's Technical Document 573 (Patterson, 1982) is presently underway and will be available in fall 1986. Carefully controlled measurements in selected geographic regions (such as various parts of the Mediterranean and the European Atlantic coast) would increase the confidence in the

database. As far as measurement techniques are concerned, the US Navy is presently conducting exploratory development of a ship-deployable air-sea temperature sensor that meets the accuracy requirements for evaporation duct height calculations. Results from this effort will be available by the end of 1986.

Reliable accounting of sea clutter effects under ducting conditions is hampered by a lack of data. Synder (1984) developed a radar sea clutter model based on a ray-optics propagation formulation combined with a semi-empirical normalized sea clutter radar cross section. A preliminary form of the model was coded for potential use in IREPS. Figures 3.5–3.7 are examples of coverage diagrams for a hypothetical 5.6-GHz radar. This model is presently not part of IREPS because it is unvalidated.

Horizontal inhomogeneities of the duct and sea-surface roughness are some of the factors contributing to signal fluctuations. Spectra and amplitudes of such fluctuations must be known for assessing bandwidth limitations (for communications) and loss of coherence (radar imaging applications). There are very few quantitative data on signal fluctuations available, which makes an accurate assessment of the above limitations very difficult.

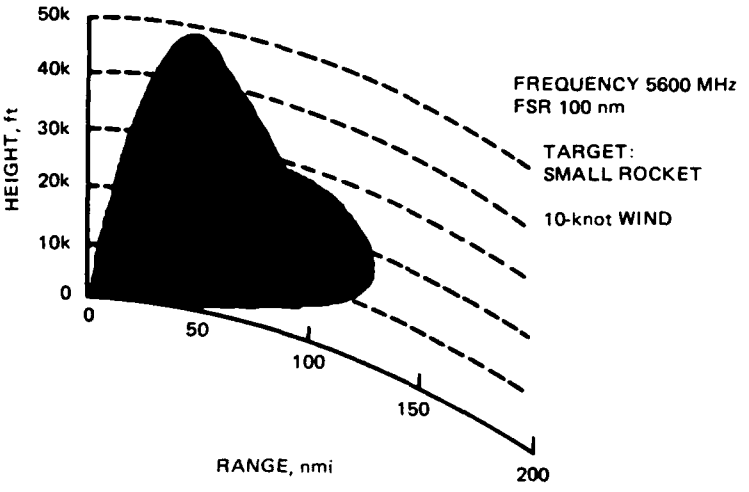

Figure 3.5. Coverage diagram for hypothetical C-band radar-standard (nonducted) atmosphere.

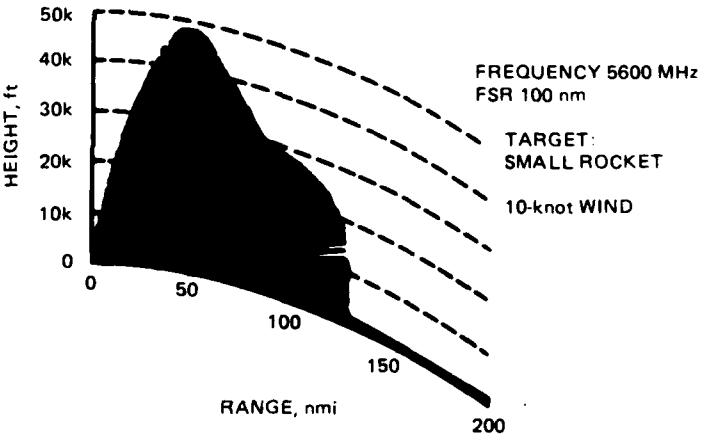

Figure 3.6. Coverage diagram for hypothetical C-band radar-surface-based duct. Duct height-300 m; refractive layer thickness-30 m.

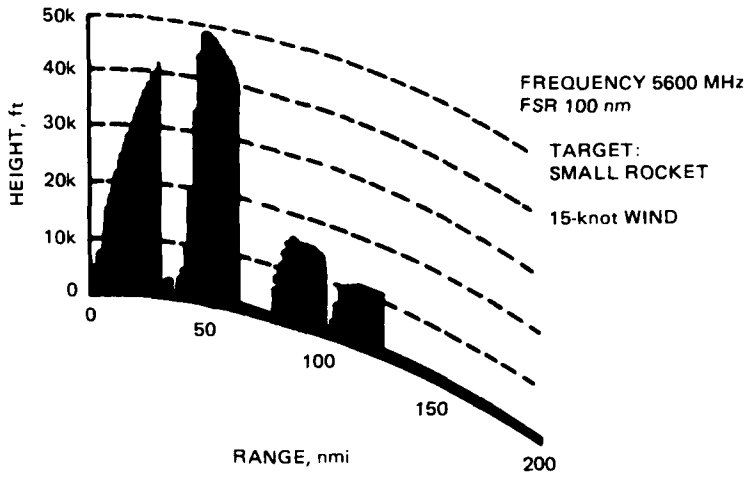

Figure 3.7. Coverage diagram for hypothetical C-band radar-surface duct. Duct height-300 m; refractive layer thickness-30 m.

3.4 SYSTEMS APPLICATIONS

The propagation phenomena discussed in section 2 apply also to the 3–30-GHz frequency band. In addition, the persistence of the evaporation ducting phenomenon has prompted various over-the-horizon radar suggestions. Specifically, radar antennas close to the ocean surface have been suggested under the incorrect assumption that coupling of energy into the evaporation duct requires antennas below the evaporation duct height. Figure 3.8a shows modified refractivity profiles for no ducting (dashed curve) and for a 47-foot duct height.

Figure 3.8b shows the vertical distribution of path loss for the two refractivity distributions, assuming a 19-nmi, 9.6-GHz over-water propagation path with one terminal at 16 feet above the water (path loss is the ratio in dB of transmitted to received power, assuming isotropic antennas). The dashed curve in figure 3.8b indicates a decrease of path loss (or an increase of signal) with height. The solid curve corresponding to the solid M-curve in figure 3.8a shows a minimum in path loss (or a maximum in received signal) at a height of about 15 feet. At this height, the signal enhancement over no-ducting conditions is 62 dB. Signal enhancements of such a magnitude emphasize the importance of the oceanic evaporation duct. (The solid curve in figure 3.8b must not be extrapolated beyond the altitude range plotted. It will not cross the "no-ducting" curve, but will, depending on horizon range, increase with altitude.) The presentation of figure 3.8b may also be used to determine antenna heights for optimum utilization of ducting conditions. For example, an antenna at a height of 64 feet would receive 11 dB less signal than an antenna at 15 feet. Nevertheless, the signal enhancement from evaporation ducting would be 30 dB for the high antenna. A fact frequently overlooked is that signal enhancements from evaporation ducting are usually encountered for all possible antenna heights on board ship. There are, however, frequency-duct height combinations for which an optimum antenna height can be determined (15 feet for 9.6 GHz in the above example). Whether a given radar antenna should be sited low for maximum ranges depends on the probability of occurrence of duct height distributions, which vary seasonally and geographically. In investigation of this question, an extensive set of over-water, over-the-horizon measurements using vertically spaced antenna was conducted (Richter and Hitney, 1972; Richter et al., 1973; Richter and Hitney, 1973; Anderson et al., 1974; Richter and Hitney, 1975). An example of one of the measurements is shown in figure 3.4(b), depicting the dB path loss difference between

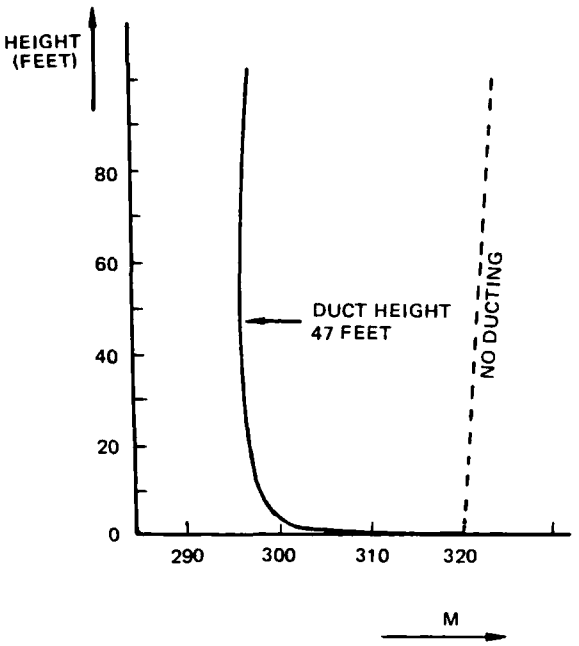

Figure 3.8a. Modified refractivity profile M for no ducting (dashed a curve) and for a 47-foot duct height (solid curve).

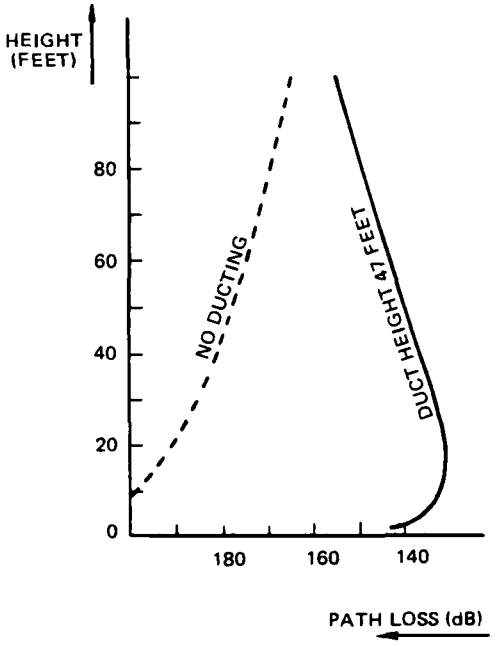

Figure 3.8b. Path loss profiles for a 9.6-GHz, 19-nmi path with a terminal height of 16 feet. The dashed curve is for no ducting and the solid curve is for a 47-foot duct height.

two vertically spaced antennas. The conclusions from these extensive measurements were that in the Southern California off-shore area for 9.6-GHz, stronger signals are received 10 percent more often on the low-sited antenna (16 feet above msl) than on the high antenna (64 feet above msl). Near Key West, Florida, the low-sited 9.6-GHz antenna (16 feet above msl) received higher signals 60 percent of the time compared to a high-sited antenna (65 feet above msl). Calculations of path loss based on meteorological measurements and observations of path loss were found to be well correlated.

Another set of radio propagation measurements in the 1-40-GHz frequency range was performed during 1972 in the Eastern Mediterranean. A propagation link between the islands of Mykonos and Naxos in the Aegean Sea was operated during four measurement periods, each lasting approximately 2 weeks. The measurements showed that evaporation ducting is an important phenomenon, in particular for frequencies above 3 GHz. For example, signal enhancements from evaporation ducting were measured 99 percent of the time at 9.6 GHz. It was determined that the evaporation duct strongly affects all shipboard antenna heights. Under conditions of strong ducting, low-sited antennas (for example, 16 feet above msl) may receive higher signals than more conventional antenna heights (for example, 64 feet above msl). For all measurements in the Mediterranean, a low-sited 9.6-GHz antenna received equal or higher signals than the high antenna 47 percent of the time. During 20 percent of the time, signals received at a low-sited 9.6-GHz antenna exceed these received on the high antenna by 10 db. If technically feasible and financially affordable, antennas of multiple heights would provide the best exploitation of the whole range of near-water propagation conditions.

The evaporation ducting effect appears to have a broad maximum in the 10–20-GHz frequency range. Atmospheric absorption and sea surface roughness apparently counteract the effectiveness of the duct expected at higher frequencies.

Simple meteorological measurements were found to be sufficient to describe ducting conditions. Horizontal homogeneity of the duct was found to be good for the propagation paths used in the investigation. Ducting effects deduced from long-term meteorological averages compared well with the actual measurements, permitting estimates of ducting conditions to be made for any oceanic area for which statistical meteorological data are available.

3.5 SYSTEMS ADAPTATIONS

The systems adaptations described in section 2.5 also apply to the 3–30-GHz frequency range. Specifically, IREPS and associated tactical decision aids have been used very successfully to adapt systems and procedures for mitigation or exploitation of evaporation ducting effects.

Attempts to develop radars that optimize use of the evaporation ducting effect have been mentioned before. These attempts have usually focused on optimum antenna height. Since optimum antenna varies with duct height, a variable antenna height is necessary, which is an important solution for a shipboard environment. However, it has been pointed out that evaporation ducting enhances detection ranges for all antenna heights. Therefore, for a wide range of duct height occurrences, it is best to site the antennas as high as possible. Anderson (1983) investigated the surface detection range capabilities of hypothetical 3, 6, 10, and 18-GHz radars of comparable performance characteristics by using worldwide ducting climatologies. Figures 3.9 and 3.10 are examples for 3- and 18-GHz radars, respectively. The figures show the percentage of time a ship target of the size of a fast frigate (FF) would be detected at ranges in excess of 60 nmi. The much higher percentage for the 18-GHz compared to the 3-GHz radar (in spite of the smaller free-space detection range for the latter) are an indication of the evaporation ducting effectiveness. Another way of presenting the above information is displayed in figure 3.11, which shows the probability of the surface-ship target detection as a function of latitude for the four frequencies analyzed.

This analysis is clearly an example of a potential adaptation of a surface surveillance radar system to the optimum use of evaporation ducting conditions.

Since atmospheric absorption, sea surface roughness, and inhomogeneities in the waveguide become more important with increasing frequency, and counteract the effectiveness of the duct to concentrate electromagnetic energy, it is felt that the frequency range between 10 and 20 GHz is optimum for exploiting evaporative ducting effects.

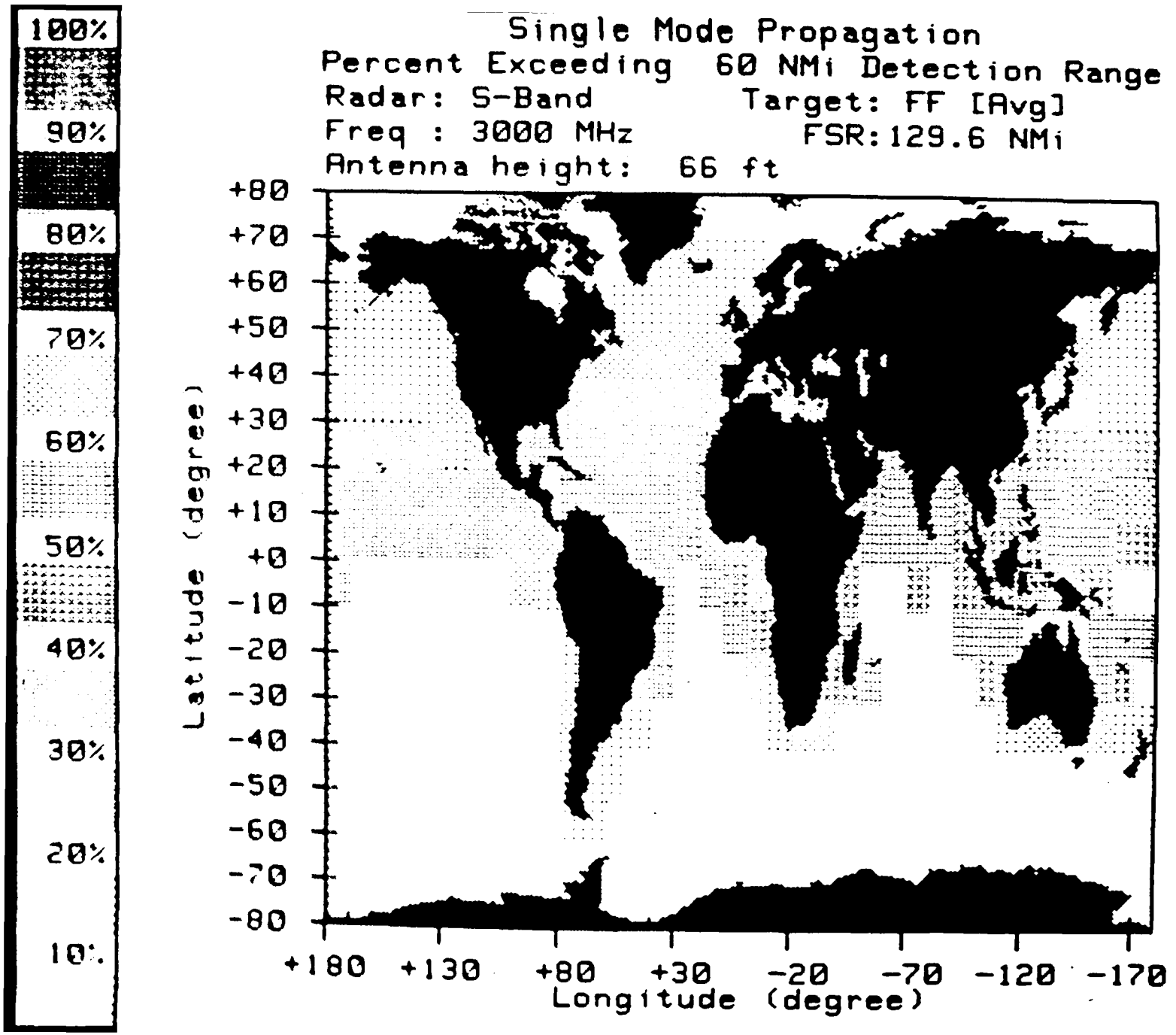
Single Mode Propagation
Percent Exceeding 60 NMi Detection Range
Radar: S-Band Target: FF [Avg]
Freq : 3000 MHz FSR:129.6 NMi
Antenna height: 66 ft
100%
90%
80%
70%
60%
50%
40%
30%
20%
10%
+80
+70
+60
+50
+40
+30
+20
+10
+0
-10
-20
-30
-40
-50
-60
-70
-80
Latitude (degree)
+180 +130 +80 +30 -20 -70 -120 -170
Longitude (degree)

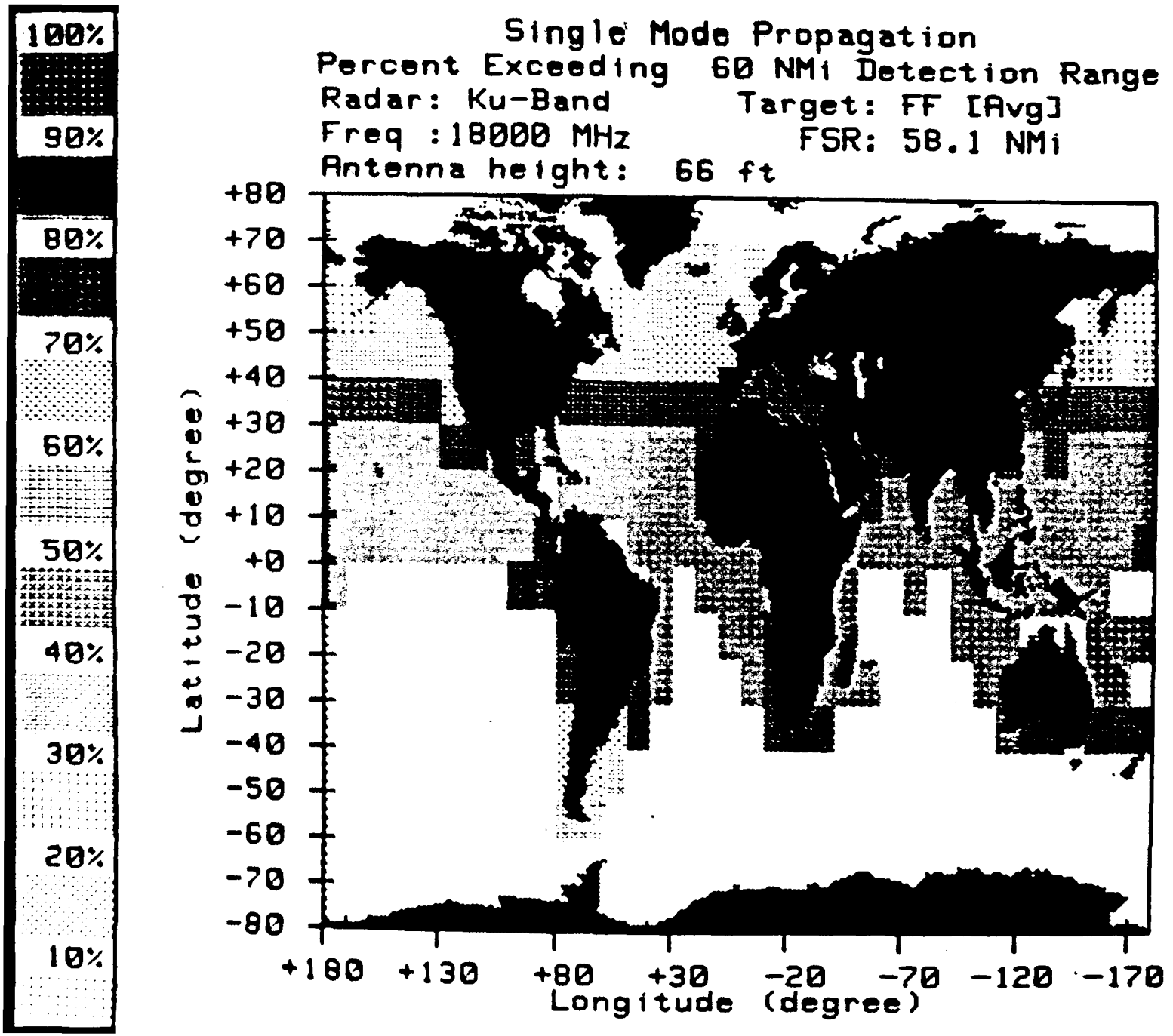
Single Mode Propagation
Percent Exceeding 60 NMi Detection Range
Radar: Ku-Band Target: FF [Avg]
Freq :18000 MHz FSR: 58.1 NMi
Antenna height: 66 ft
100%
90%
80%
70%
60%
50%
40%
30%
20%
10%
Latitude (degree)
+80
+70
+60
+50
+40
+30
+20
+10
+0
-10
-20
-30
-40
-50
-60
-70
-80
+180 +130 +80 +30 -20 -70 -120 -170
Longitude (degree)

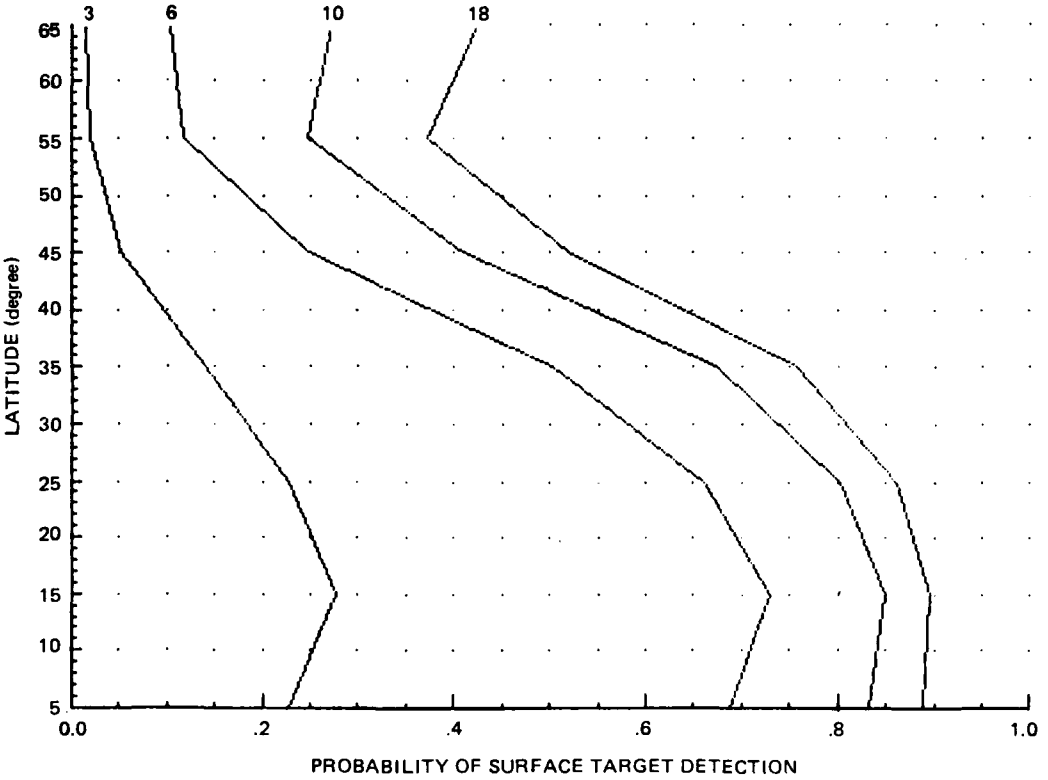

Figure 3.11. Geographic influence of the evaporation duct on shipboard radar surface-target detection capabilities. The target is well beyond the normal horizon and the increased detection range is attributable solely to the evaporation duct. Predictions are for four radar frequencies: 3, 6, 10, and 18 GHz.

4. NEAR-WATER PROPAGATION EFFECTS ON SYSTEMS AT EHF (30-300 GHz)

4.1 NORMAL PROPAGATION

Normal attenuation further increases throughout the 30–300-GHz frequency band. Three strong gaseous resonances occur in this region (see figure 3.1) with associated absorption maxima (molecular oxygen resonances around 60 and 120 GHz and a water vapor resonance around 183 GHz). The refractive index can no longer be considered nondispersive. A number of models have been developed that deal with the absorption and dispersion properties affecting propagation [Waters, 1976; Zrazheviskiy, 1976; Falcone et al., 1982 (FASCODE); Duncan and Steinhoff, 1982 (EOSAEL); Liebe, 1981; Liebe, 1983; Liebe, 1984; Liebe, 1985; Liebe and Dillon 1969; Liebe et al., 1977; Liebe et al., 1985].

Figure 4.1 is taken from Liebe et al., (1985) and shows sea-level attenuation and dispersive delay for a variety of humidity (including fog) conditions. Figure 4.1a applies to $T = 5°C$ and a liquid water content of $W = 0.1$ g/m^3; figure 4.1b applies to $T = 25°C$ and no aerosols present. Figure 4.1a–b illustrates the strong variability of attenuation and phase delay throughout the EHF band. An accurate knowledge of the atmospheric parameter is crucial to accurate propagation predictions. The most convenient way of obtaining accurate

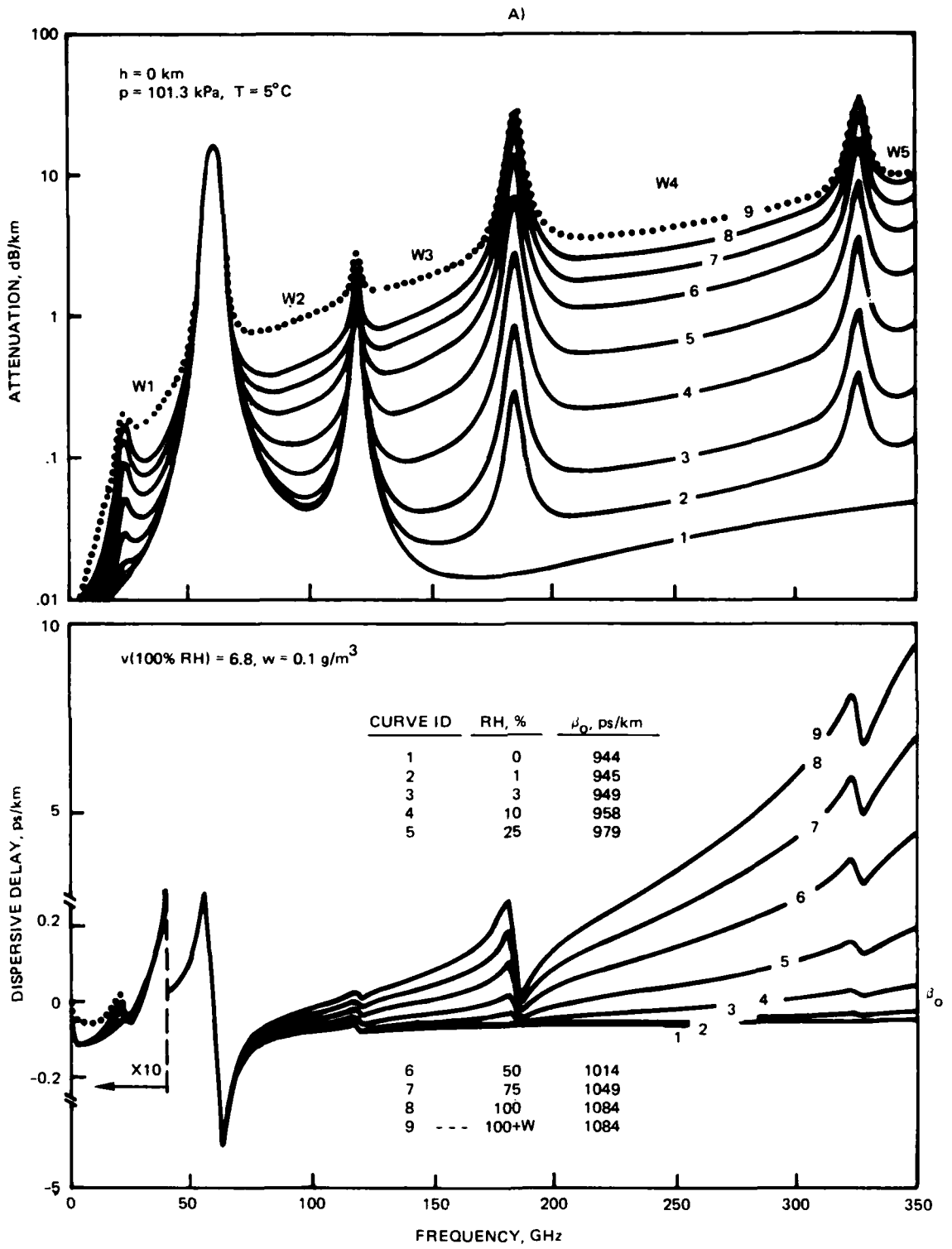

Figure 4.1. Predicted specific attenuation and α and dispersive delay β for moist air (0-100% RH) at sea level, including simulated fog conditions (w = 0.1) with roughly 300 m visibility. Five atmospheric millimeter-wave window ranges are marked W1 to W5 [$\beta_o = 3.336\ N_o$, refractive delay: a) T = 5°C and w = 0.1; from Liebe et al., (1985)].

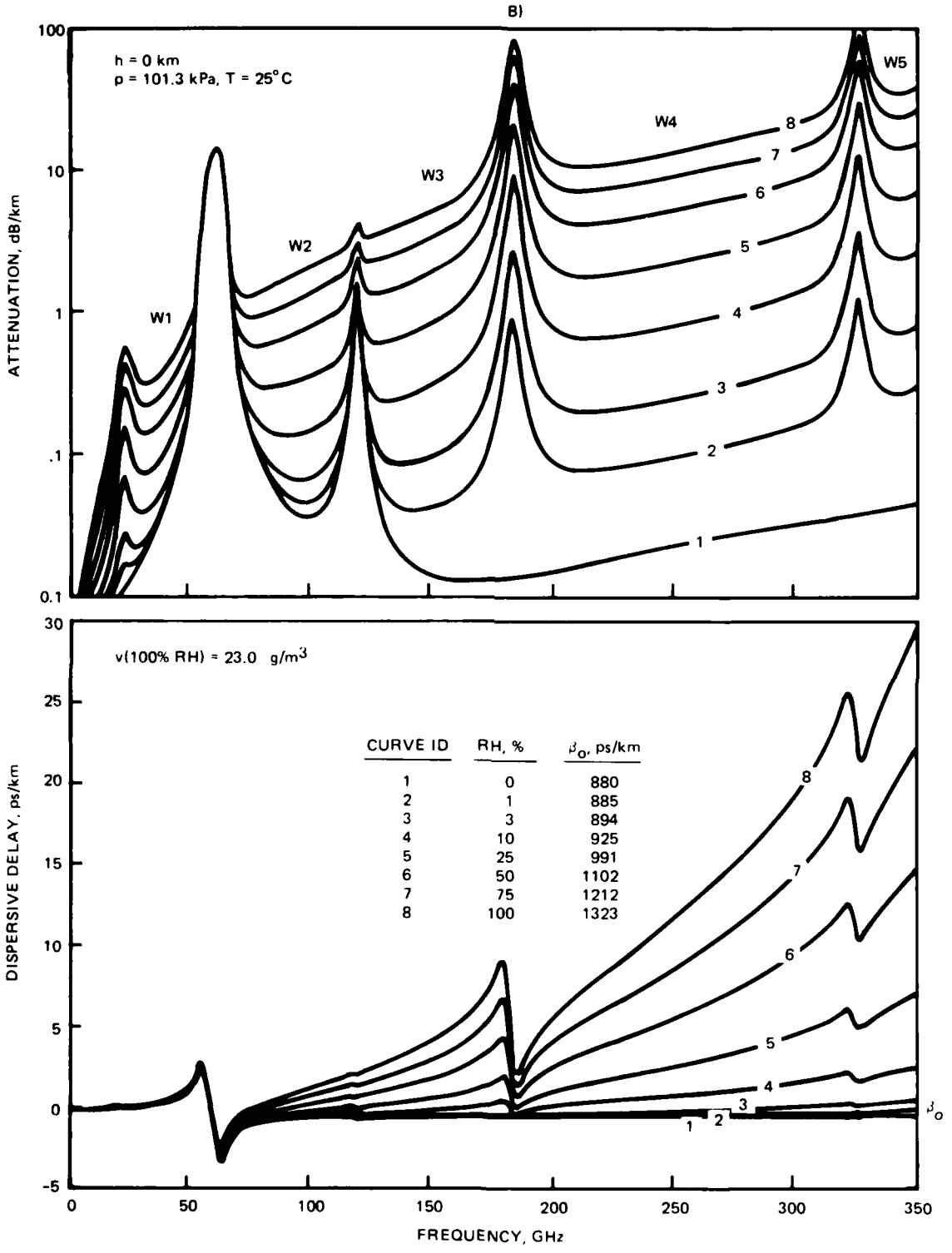

Figure 4.1. (Continued): b) T = 25°C and w = o.

propagation parameter calculations is the use of one of the many computer programs developed for this purpose. Figure 4.2a–b is an example of Liebe's millimeter propagation model (MPM) programmed for an IBM PC.

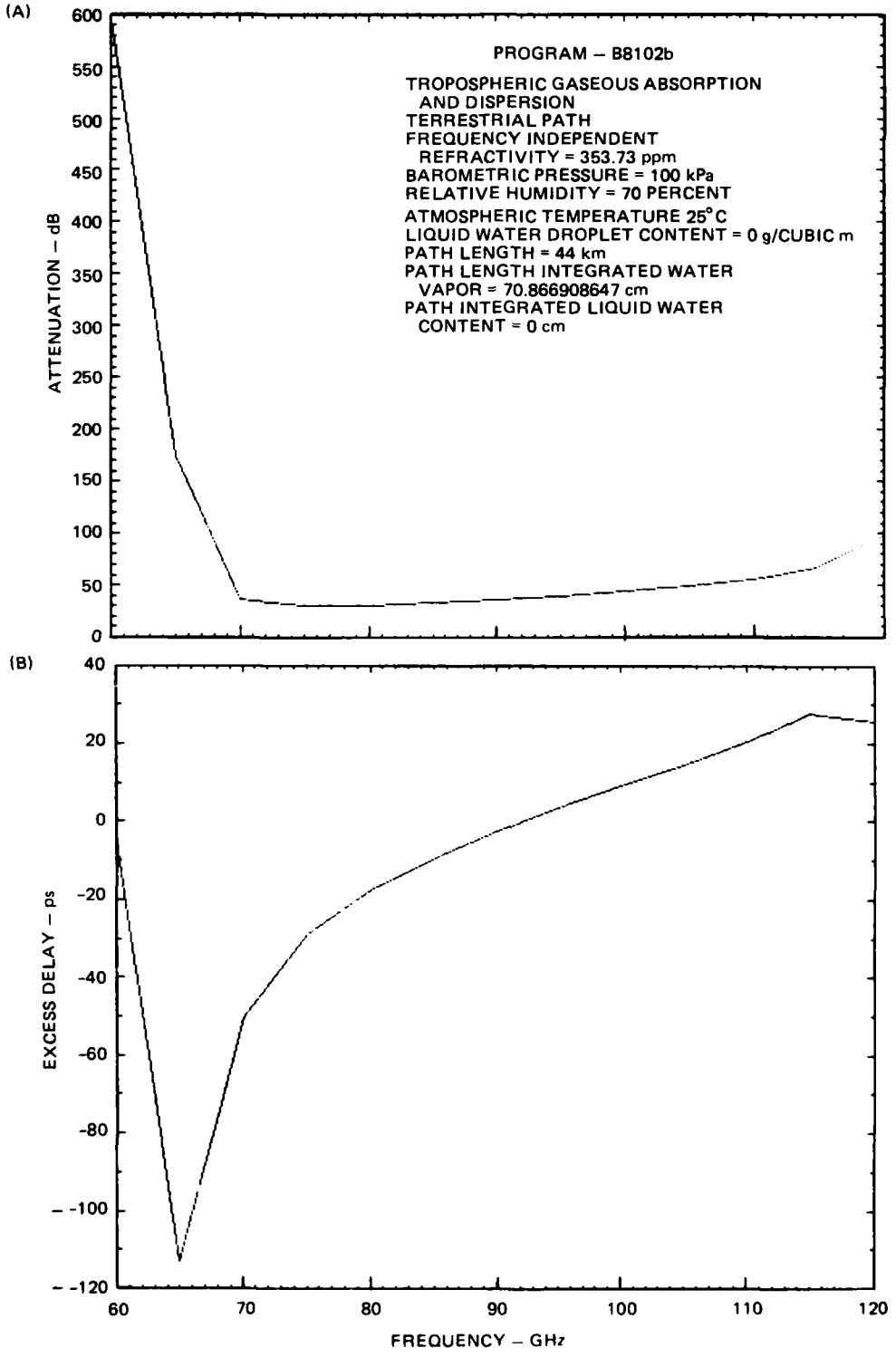

Figure 4.2. Attenuation (a) and excess path delay (b) for a 44-km propagation path.

Atmospheric turbulence may cause propagation effects such as amplitude fluctuations, phase front distortion, and variations in angle of arrival. For a quantitative assessment of turbulent effects, the refractive structure function constant C_n^2 must be determined. (Tatarski, 1961; Clifford and Strohbehn, 1970; Ishimaru, 1972; Ott and Thompson, 1978; Cole et al., 1978; Hill and Clifford, 1981; Liebe et al., 1985.)

The effect of attenuation by rain is included in some of the propagation modeis (e.g., Falcone et al., 1979) by using Mie theory and dropsize distributions (which can be related to rain rate). As one can see from figure 3.1, rain quickly becomes the dominating attenuation effect in the EHF band.

4.2 ANOMALOUS PROPAGATION

The propagation anomalies described in chapters 2.2 and 3.2 also apply to the EHF band. However, the effectiveness of atmospheric ducts may be reduced by molecular absorption, hydrosols, and inhomogeneities in the waveguide, as illustrated by figure 4.3.

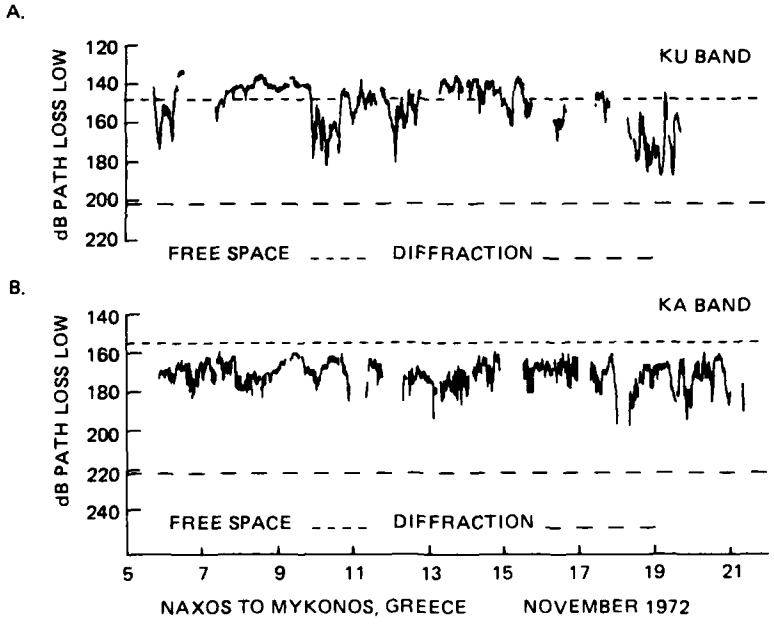

Figure 4.3. Pathloss measurements at 18 GHz (Ku band) and 37.4 GHz (Ka band). Path length: 19 nmi; antenna heights: 4.3 and 4.6 m (18 GHz) and 3.7 and 5.3 m (37.4 GHz).

During the 2-week measurement period, evaporation ducting caused strongly enhanced signals at both frequencies. For a significant portion of this period, the 18-GHz signals exceeded free-space values, in contrast to the 37.4-GHz signals, which never reached free-space levels even though calculations for the duct heights encountered indicated higher signals. These calculations were done for a smooth ocean surface. When this assumption in the calculation was changed by introducing an RMS wave height of 0.3 m (corresponding to the prevailing wind conditions of 10–13 knots), the calculated signal levels agreed with the measured values (Richter and Hitney, 1975).

In the second atmospheric window in the EHF band (labeled W2 in figure 4.1), propagation measurements are sparse and usually are line-of-sight paths. Evaporation ducting should influence propagation in this window significantly. Figure 4.4 shows 94-GHz calculations that indicate large signal levels. For example, 80-dB signal enhancements are calculated at a range of 30 km for the antenna geometries assumed. The actual expected signals should be smaller through effects of sea-surface roughness and inhomogeneities in the guide.

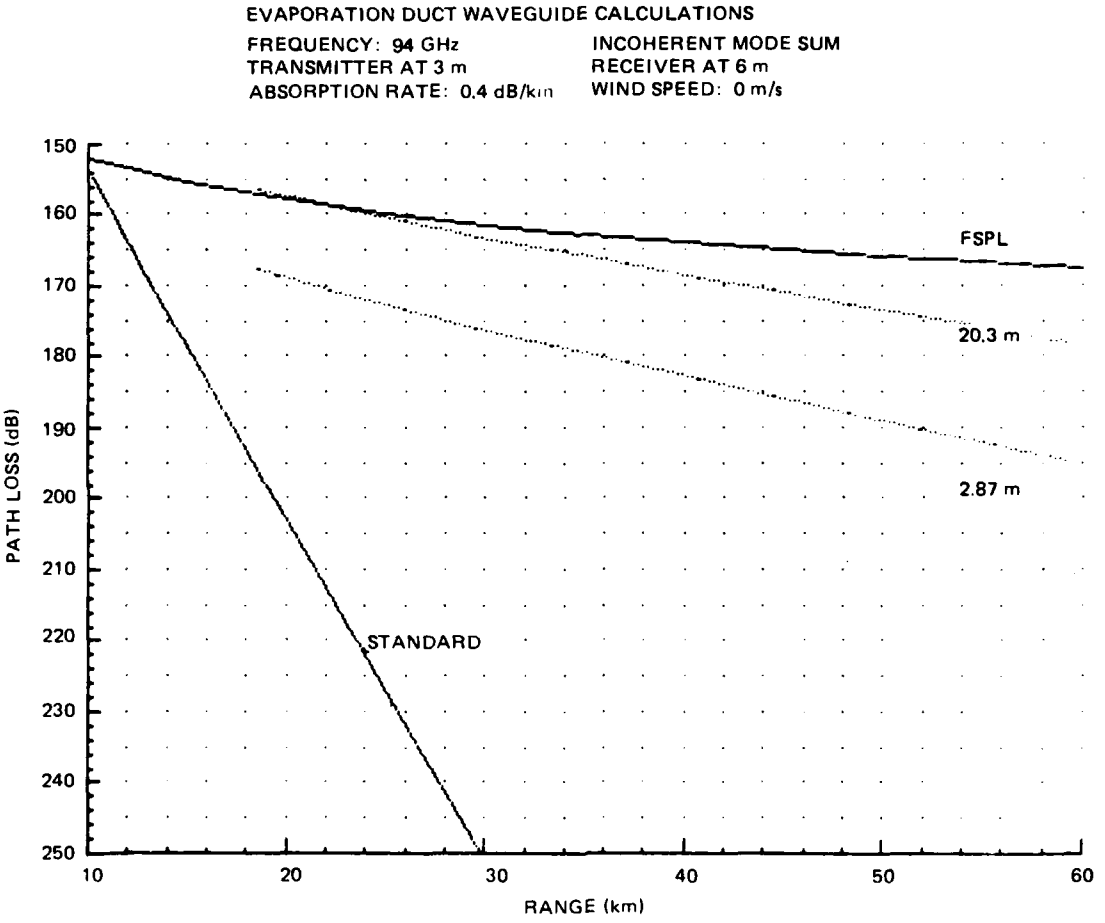

Figure 4.4. Pathloss versus range for evaporation duct heights of 2.87 and 20.3 m, assuming smooth seas. Transmitter at 3 m above MSL, receiver at 6 m above MSL.

4.3 DATA GAPS TO BE FILLED

With the exception of a few line-of-sight measurement, little anomalous propagation information, particularly over the ocean, exists in windows 2, 3, 4 (figure 4.1) of the EHF band. A specially urgent need is good measurements in window 2 (around 95 GHz), since this is the most likely frequency region for future systems. One propagation experiment is

planned for 1986 in the Southern California coastal area. It consists of a 40-km, 94-GHz link with 10-m and 5-m antenna heights. Similar measurements should be performed in other geographic areas.

4.4 SYSTEMS APPLICATIONS

The EHF band is attractive for systems applications for a number of reasons. First, small wavelengths facilitate small antenna beamwidths. Applications for which small antenna beamwidths are desirable are covert communications and terminal guidance systems with multipath (sea-reflected) suppression. Second, the EHF band offers much better fog and haze penetration capabilities than the infrared or visible band (for which narrow beams are easily achieved). Third, because of the high carrier frequencies in the EHF band, high bandwidths and consequently high data rates can be achieved. Fourth, the EHF band is not as congested as the lower-frequency bands, resulting in less mutual interference. Fifth, operation in the absorption peaks (e.g., 60 GHz) further increases covertness. An example would be communications on aircraft carrier flight decks. Sixth, the water-vapor resonance at 183 GHz may be useful for remote water-vapor sensing techniques. For all the above reasons, there are a number of EHF communications, radar, sensor, and weapon systems that have been proposed or are under development. For their proper functioning in a marine environment, more confidence in our ability to assess propagation conditions is urgently needed.

4.5 SYSTEMS ADAPTATIONS

The major requirement for systems adaptation is the development of an accurate assessment technology for the propagation environment. Before this can be done, proper mathematical models must be developed and experimentally validated. Once such a capability exists, tactical decision aids may be developed that recognize and exploit the propagation environment. For example, systems are envisioned that have both IR/optical and mm-wave capabilities. Reliable, possibly automated, decision aids are then necessary to select the propagation band best suited for the environmental conditions encountered.

5. REFERENCES

Anderson, K.D., H.V. Hitney, D.R. Jensen, and J.H. Richter, (1974), Propagation Measurements Between San Clemente and San Nicolas Islands, NELC Technical Note 2768.

Anderson, K.D., (1982), Inference of Refractivity Profiles by Satellite-to-Ground RF Measurements, Radio Sci., vol 17, No 3, pp 653–663.

Anderson, K.D., (1983), Surface-Search Radar Performance in the Evaporation Duct: Global Predictions, NOSC TR 923, Rev A.

Burk, S.D., (1977), The Moist Boundary Layer With a Higher Order Turbulence Closure Model, J. Atmos. Sci., vol 34, pp 629–638.

Burk, S.D., (1980), Refractive Index Structure Parameters: Time Dependence Calculations Using a Numerical Boundary-layer Model, J. Appl. Meteor., vol 19, pp 562–576.

C.C.I.R., (1976), Conclusions of the Interim Meeting of Study Group 5 (Propagation Non-Ionized Media), Doc 5/142-E, 26 April 1976.

Clifford, S.F., and J.W. Strohbehn (1970), The Theory of Microwave Line-of-Sight Propagation Through a Turbulent Atmosphere, IEEE Trans. Ant. Prop. Ap-18, No. 2, pp 264–274.

Cold, R.S., K.L. Ho, and N.D. Mavrokoukoulakis, (1978), The Effect of the Outer Scale of Turbulence and Wavelength on Scintillation Fading at Millimeter Wavelengths, IEEE Trans. Ant. Prop. AP-26, No. 1, pp 10–19.

Crane, R.K. (1967), Coherent Pulse Transmissions Through Rain, IEEE Trans. AP-15, pp 252–256.

Duncan, L.D., and R.G. Steinhoff (Ed.), (1982), EOSAEL 80 Users Manual, vol II, Rep. ASL-TR-0107, USAERCDC Atmos. Sci. Lab., White Sands Missile Range, N.M.

Falcone, V.J., L.W. Abreu, and E.P. Shettle, (1979), Atmospheric Attenuation of Millimeter Waves, Models and Computer Code, AFGL-TR-79-0253, Air Force Geophysics Laboratory, Bedford, MA 01731.

Falcone, V.J., Jr., L.W. Abreu, and E.P. Shettle, (1982), Atmospheric Attenuation in the 30 to 300 GHz Region Using RADTRAN and MWTRAN, Proc. Soc. Photo Opt. Instrum. Eng., 337, pp 62–66.

Freehafer, J.E., (1951), Tropospheric Refraction, Propagation of Short Radio Waves, D.E. Kerr (Ed.), New York: McGraw-Hill, pp 9–22.

Glevy, D.F., (May 1976), An Assessment of Radio Propagation Affected by Horizontal Changes in Refractivity, Naval Electronics Lab. Cen. Tech. Note 3153.

Gossard, E.E., (1977), Refractive Index Variance and its Height Distribution in Different Air Masses, Radio Sci., vol 12, pp 89-105.

Gossard, E.E., (1978), The Distribution of Radio Refractive Index Structure Parameter in Boundary Layers Undergoing Spatial or Temporal Transition, Radio Sci., vol 13, pp 255-259.

Gossard, E.E., (1978), The Height Distribution of Refractive Index Structure Parameters in an Atmosphere Being Modified by Spatial Transition at its Lowest Boundary, Radio Sci., vol 13, pp 489-500.

Gossard, E.E., R.B. Chadwick, W.D. Neff, and K.P. Moran, (1982), The Use of Ground-based Doppler Radars to Measure Gradients, Fluxes, and Structure Parameters in Elevated Layers, J. Appl. Meteor., vol 21, No. 2.

Hattan, C.P., W.L. Patterson, H.V. Hitney, R.A. Paulus, K.D. Anderson, and G.E. Lindem, (1983), IREPS Revision 2.2 User's Manual, Naval Ocean Syst. Cen. Tech. Doc. 659.

Helvey, R.A., (1983), Radiosonde Errors and Spurious Surface Ducts, Proc. IEEE, vol 130, Part F., No. 7.

Hill, R.J., and S.F. Clifford, (1982), Contribution of Water Vapor Resonances to Fluctuations of Refraction and Absorption for Sub mm Through cm Wavelengths, Radio Sci. 16, No. 1, pp 77-82.

Hitney, H.V., and J.H. Richter, (1976), Integrated Refractive Effects Prediction System (IREPS), Nav. Eng. J., vol 88, No. 2, pp 257-262.

Ishimaru, A., (1972), Temporal Frequency Spectra of Multifrequency Waves in Turbulent Atmosphere, IEEE Trans. Ant. Prop. AP-20, pp 10-19.

Jeske, H., (1971), The State of Radar-Range Prediction Over Sea, AGARD Conf. Proc., 70(2), pp 50.1-50.10.

Liebe, H.J., and T.A. Dillon, (1969), Accurate Foreign-Gas-Broadening Parameters of the 22-GHz H_2O Line From Refraction Spectroscopy, J. Chem. Phys., 50(2), pp 727-732.

Liebe, H.J., G.G. Gimmestad, and J.D. Hopponen, (1977), Atmospheric Oxygen Microwave Spectrum-Experiment Versus Theory, IEEE Trans. Antennas Propag., AP-25(3), pp 327-355.

Liebe, H.J., (1981), Modeling Attenuation and Phase of Radio Waves in Air at Frequencies Below 1000 GHz, Radio Sci. 16(6), pp 1183-1199.

Liebe, H.J., (1983), Atmospheric EHF Window Transparencies Near 35, 90, 140, and 220 GHz, IEEE Trans. Antennas Propag., AP-31(1), pp 127-135.

Liebe, H.J., (1984), The Atmospheric Water Vapor Continuum Below 300 GHz, Int. J. Infrared Millimeter Waves, 5(2), pp 207-227.

Liebe, H.J., (1985), An Updated Model for Millimeter Wave Propagation in Moist Air, Radio Science 20(5), pp 1069-1089.

Liebe, H.J., K.C. Allen, G.R. Hand, R.H. Espeland, and E.J. Violette, (1985), Millimeter Wave Propagation in Moist Air: Model Versus Path Data, NTIA Rep. 85-171, Natl. Telecommun. and Inform. Admin., Boulder, Colo.

Monin, A.S., and A.M. Obukhov, (1954), Basic Laws of Turbulent Mixing in the Ground Layer of the Atmosphere, Tr. Geofiz. Akad. Nauk. SSSR, 151, pp 163-187.

Ott, R.T, and M.C. Thompson, Jr., (1978), Atmospheric Amplitude Spectra in an Absorption Region, IEEE Trans. Ant. Prop. AP-26, No. 2, pp 329-332.

Patterson, W.L., (1982), Climatology of Marine Atmospheric Effects, NOSC TD 573.

Patterson, W., (1985), Comparison of Evaporation Duct and Path Loss Models, Radio Science, 20(5), pp 1061-1068.

Paulus, R.A., (1985), Practical Application of an Evaporation Duct Model, Radio Science, 20(4), pp 887-896.

Richter, J.H., (1969), High Resolution Tropospheric Radar Sounding, Radio Sci., vol 4, No. 12, pp 1261-1268.

Richter, J.H., and H.V. Hitney, (1972), Antenna Heights for Optimum Utilization of the Oceanic Surface Evaporation Duct, Part I: Results from the Pacific Measurements, NELC Technical Note 2031.

Richter, J.H., and H.V. Hitney, (1973), Antenna Heights for Optimum Utilization of the Oceanic Surface Evaporation Duct, Part II: Results from the Key West Measurements, NELC Technical Note 2371.

Richter, J.H., and H.V. Hitney, (1973), Antenna Heights for Optimum Utilization of the Oceanic Surface Evaporation Duct, Part III: Results from the Mediterranean Measurements, NELC Technical Note 2569.

Richter, J.H., H.V. Hitney, K.D. Anderson, and M.L. Phares, (1973), Propagation Measurements of 37 GHz in the Oceanic Surface Evaporation Duct, NELC Technical Note 2422.

Richter, J.H., and H.V. Hitney, (1975), The Effect of the Evaporation Duct on Microwave Propagation, Tech. Rep. 1949, Nav. Electron. Lab. Cent., San Diego, Calif.

Rotheram, S., (1977), Radiowave Range Prediction Over the Sea in Evaporation Ducting Conditions, Tech. Rep. 77/37, Marconi Res. Lab., Great Baddow, Chelmsford, England.

Skolnik, M.I., (1980), Introduction into Radar Systems, McGraw-Hill Book Company, New York.

Snyder, F.P., (1984), A Radar Sea Clutter Model for Atmospheric Ducting Conditions, NOSC TD 721.

Tatarski, V.I., (1961), Wave Propagation in a Turbulent Medium, translated from Russian by R.A. Silverman, McGraw-Hill, New York.

Waters, J.R., (1976), Absorption and Emission by Atmospheric Gases, in Methods of Experimental Physics, vol 12B, edited by M.L. Meeks, chap. 2.3, Academic Press, New York.

Zrazheviskiy, A.Y., (1976), Method of Calculating Atmospheric Water Vapor Absorption of Millimeter and Submillimeter Waves, Radio Eng. Electron. Phys., 21(5), pp 31-36.

Technical Notes are internal working documents not given general distribution outside NELC or NOSC. For further information about these references, contact the author(s).

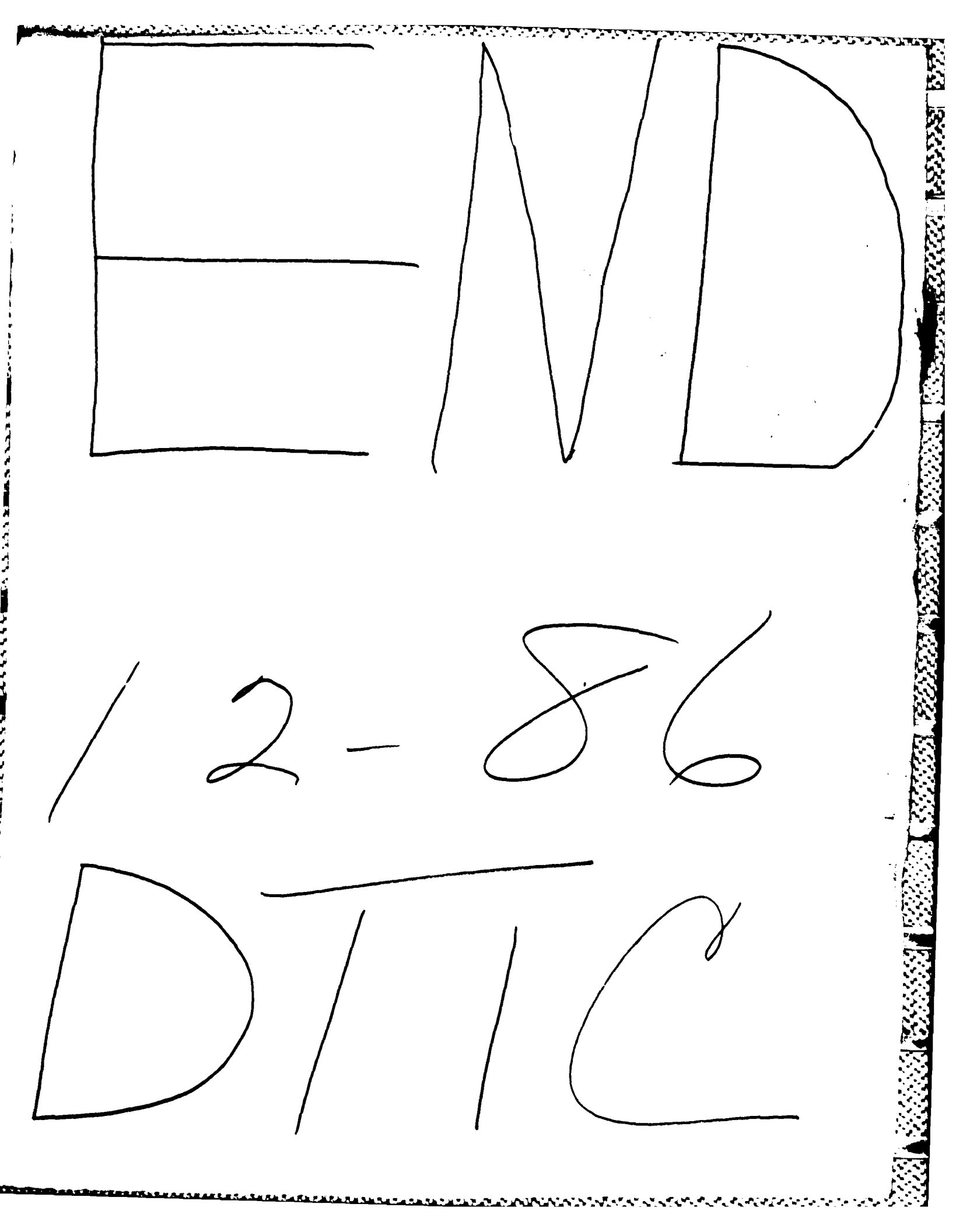
END
12-86
DTIC